Upgrade of ambient pressure X-ray photoelectron spectroscopy system at SPring-8 BL07LSU

Susumu Yamamoto[1,2], Takanori Koitaya[3], Iwao Matsuda[4], and Jun Yoshinobu[4]

[1] *International Center for Synchrotron Radiation Innovation Smart (SRIS), Tohoku University*

[2] *Institute of Multidisciplinary Research for Advanced Materials (IMRAM), Tohoku University*

[3] *Department of Chemistry, Graduate school of Science, Kyoto University*

[4] *The Institute for Solid State Physics, The University of Tokyo*

Introduction

Operando spectroscopy allows direct observation of materials and devices under actual operation conditions to find a correlation between structure and function in materials. As *Operando* spectroscopy in the soft X-ray region, we developed ambient pressure X-ray photoelectron spectroscopy (AP-XPS) system at the high-brilliance soft X-ray beamline BL07LSU of SPring-8 [1, 2]. We have been promoting research on *operando* observation of catalytic reactions. The limitations of the AP-XPS system were revealed by our past experiments: 1) low maximum gas pressure, and 2) low temporal resolution. As for 1) low maximum gas pressure, the maximum gas pressure in the AP-XPS measurements was limited to about 20 mbar for bulk samples. The low maximum gas pressure leads to low reactivity and selectivity in catalytic reactions. Regarding 2) low temporal resolution, the temporal resolution of the present AP-XPS system was limited to sec~min.

Therefore, in our long-term project, we set two goals to upgrade the AP-XPS system at SPring-8 BL07LSU: 1) Increase the maximum gas pressure, and 2) development of picosecond time-resolved AP-XPS system.

Results and discussion

1) Increase the maximum gas pressure in AP-XPS

The XPS signal attenuation in a gas phase is proportional to $\exp(-z\sigma p)$, where z is the distance between the sample and the entrance nozzle of an electron spectrometer, σ scattering cross section of photoelectrons, p gas pressure. In order to mitigate the XPS signal attenuation, one effective approach is to keep z small. When the distance z is small, however, the local gas pressure on the sample surface is decreased due to the differential pumping through the entrance nozzle. To avoid the decrease of local gas pressure, the opening of the entrance nozzle needs to be decreased.

In the past AP-XPS system, the diameter of the nozzle opening was 300 μm, and the distance z was set at ~300 μm. We developed a new nozzle with the opening diameter of 50 μm. The nozzle body was manufactured by an electroforming technique at Institute for Molecular

Science. The opening hole was made by a focused ion beam. The distance z was set at ~100 μm. Using the new 50 μm nozzle, we have succeeded in measuring Au 4f XPS spectra in the presence of 100 mbar N_2 gas. Therefore, the maximum gas pressure of the AP-XPS system was improved from 20 mbar to 100 mbar. After the improvement of the maximum gas pressure, the AP-XPS system was used to study various systems such as H_2 absorption process in Pd alloys, partial oxidation of CH_4, and CO_2 hydrogenation reactions on catalyst surfaces.

2) Development of picosecond time-resolved AP-XPS system

We have developed the picosecond time-resolved AP-XPS system that combined AP-XPS with femtosecond optical laser. To match the repetition rate of soft X-ray with that of optical laser, the soft X-ray chopper was installed at the beamline. The photodiode mounted on an XYZ stage was newly introduced to an analysis chamber to determine time zero in a pump-probe delay time. On a p-type Si(100) substrate covered with natural oxide (SiO_2/p-Si(100)), temporal variation of Si 2p XPS peak energy due to surface photovoltage effect was observed both in ultrahigh vacuum and in CO_2 gas atmosphere. Furthermore, we succeeded in observing the photoexcitation dynamics on α-Fe_2O_3(0001) surface in a water vapor gas atmosphere.

REFERENCES

[1] S. Yamamoto *et al.*, *Synchrotron Radiat. News* **35**, 19-25 (2022).

[2] S. Yamamoto *et al.*, *Journal of the Japanese Society for Synchrotron Radiation Research* **35**, 182-190 (2022). (in Japanese)

DEVELOPMENT OF SOFT X-RAY MICROSCOPY SYSTEM AND ITS APPLICATION TO MEASUREMENT OF MAMMALIAN CELLS

Yoko TAKEO,[1,2] Kai SAKURAI,[3] Noboru FURUYA,[3] Kyota YOSHINAGA,[3] Takenori SHIMAMURA,[4] Satoru EGAWA,[4] Hisao KIUCHI,[1] Hidekazu MIMURA,[4] Haruhiko OHASHI,[2] Yoshihisa HARADA,[1] Mari SHIMURA,[5,6] and Takashi KIMURA[1]

[1]*The Institute for Solid State Physics, The University of Tokyo*

[2]*Japan Synchrotron Radiation Research Institute*

[3]*Department of Applied Physics, School of Engineering, The University of Tokyo*

[4]*Department of Precision Engineering, School of Engineering, The University of Tokyo*

[5]*RIKEN, SPring-8 Center*

[6]*Research Institute, National Center for Global Health and Medicine*

X-ray microscopy has a wide range of applications in science due to its high spatial resolution and variety of analytical techniques. Ptychography provides a particularly high spatial resolution by reconstructing the sample image using phase recovery calculations[1, 2]. The combination of ptychography and spectroscopy in the soft X-ray region is promising for investigating samples with light-element-rich heterogeneous structures. For example, in the combination of soft X-ray ptychography with X-ray absorption spectroscopy, mapping the chemical state of magnetic nanoparticles in bacteria[3] and the visualization of the cathode degradation mechanism of the lithium-ion batteries[4] have been demonstrated.

Ptychography, a lensless imaging technique, has rapidly developed over the past decade. By reconstructing sample images from multiple coherent diffraction patterns using iterative phase retrieval algorithms, it is possible to obtain high spatial resolution images that are not affected by the performance of X-ray optics, such as fabrication accuracy. In addition, the phase retrieval of coherent diffraction patterns allows the acquisition of both conventional absorption images and phase images, which is a significant advantage when measuring samples with high X-ray transmittance, such as biological cells.

Combining ptychography-based imaging with X-ray fluorescence analysis allows for investigating the correlation between microstructure and element distribution. In the soft X-ray region, ptychography and X-ray fluorescence microscopy systems have been developed using zone plates as illumination optics. Previous results have demonstrated their usefulness, such as the visualization of the chemical state of lithium-ion battery materials and the internal microstructures of magneto bacteria and mammalian cells. Although zone-plate-based optical systems offer the advantages of simplicity and small focus size, they also suffer from problems such as chromatic aberration and short working distances. Illumination optics using total reflection X-ray mirrors have excellent features, such as long working distances, suitable for developing instruments combined with detectors for X-ray photography and X-ray fluorescence analysis. In addition, total reflection mirrors are achromatic, so changing the X-ray wavelength does not affect the focusing properties and are thus well-suited for wavelength scans without the need to readjust the optical system.

In this study, we developed a new soft X-ray microscopic imaging system that combines soft X-ray ptychography and an X-ray fluorescence microscope, using an optical illumination system based on a total reflection Wolter mirror[7]. Figure 1 shows the Shematic illustration of the system called CARROT (Coherent Achromatic Rotational Reflective Optics for pTychography.).We measured mammalian cells as samples and visualized the internal structure with soft X-rays by the absorption and phase shift. We successfully captured sub-micrometer-scale subtle changes in cellular structure due to drug administration by taking advantage of the high-resolution images provided by ptychography (Figure 2). Furthermore,

we demonstrated that it is possible to map the elemental distribution inside the cells using X-ray fluorescence by seamlessly changing the irradiation wavelength from the ptychography measurement. We find a correlation between the internal structure and the elemental distribution inside the cells.

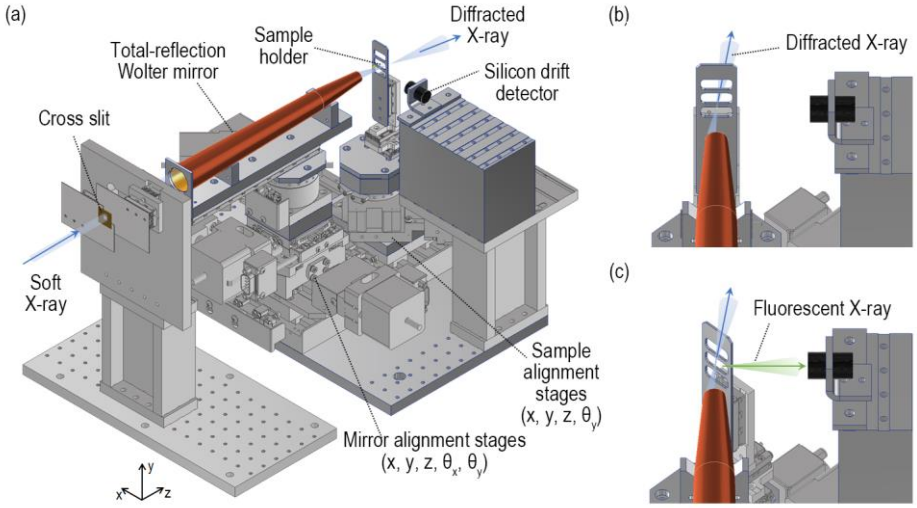

Figure 1 Schematic illustration of the CARROT system. (a) The overall structure inside the vacuum chamber. (b) Ptychography measurement mode. (c) X-ray fluorescence imaging mode.

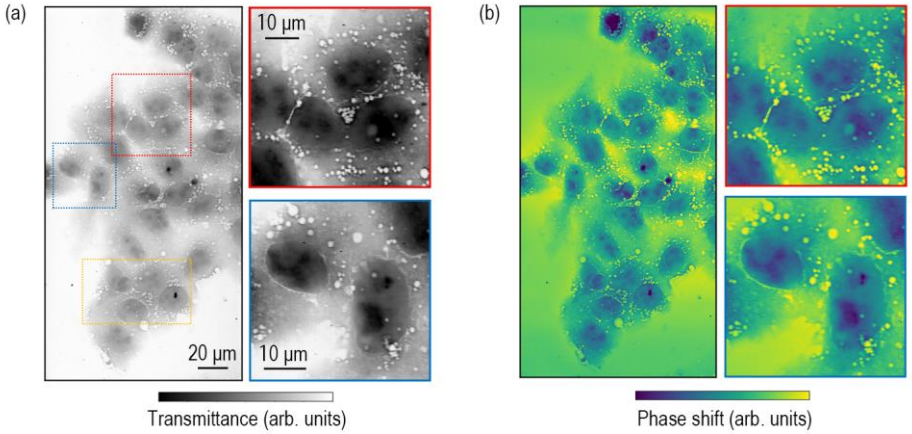

Figure 2 Soft X-ray ptychography measurement of HepG2 cells (DMSO treated). Reconstructed absorption (a) and phase shift (b) images. The magnified images shown in the right panels corresponding to the dotted colored rectangles shown in (a).

REFERENCES

[1] A. M. Maiden, J. M. Rodenburg, Ultramicroscopy, 109 (10), 1256 (2009).
[2] P. Thibault, et al., Science, 321, 379 (2008).
[3] X. Zhu, et al. Proc. Natl. Acad. Sci. , 113 (51) E8219 (2016).
[4] T. Sun, et al., ACS Nano, 15, 1475 (2021).
[5] Y. Takeo, et al., Appl. Phys. Lett. 117, 151104 (2020)
[6] T. Kimura, et al., Opt. Express, 30(15), 26220 (2022).
[7] Y. Takeo, et al., J. Electron Spectrosc. Relat. Phenom., accepted.

CHANGES OF INTRACELLULAR STRUCTURES BY SOFT X-RAY MICROSCOPY SYSTEM OF CT-PTYCHOGRAPHY

Mari Shimura,[1,2] Yoko Takeo,[3,4] Kai Sakurai,[5]
Haruhiko OHASHI,[4,1] Hidekazu Mimura,[6] and Takashi Kimura,[3]

[1]RIKEN, SPring-8 Center
[2]National Center for Global Health and Medicine
[3]The Institute for Solid State Physics, The University of Tokyo,
[4]Japan Synchrotron Radiation Research Institute
[5]Department of Applied Physics, School of Engineering, The University of Tokyo
[6]Department of Precision Engineering, School of Engineering, The University of Tokyo

We had been applied biological samples such as culture cells and medical samples using synchrotron hard x-ray by establishing a scanning x-ray fluorescence microscopy (SXFM) since more than 15 years ago and figured out much evidence that synchrotron x-ray has a potential ability that we have never seen with visible light and electron microscopies [1, 2]. Imaging proteins has been well developed and established in biological and medical fields by visible light microscopies with a labelling technology such as fluorescence; however, synchrotron x-ray microscopy reminds us of a different point of view that proteins are just a part of the cellular contents. In these days, we could obtain an opportunity to apply soft x-ray microscopy system of ptychography with x-ray absorption spectroscopy established at BL07LSU to biological samples [3].

In this study, we prepared a common SiN basement which is available for both SXFM at BL29XU and CARROT at BL07LSU [3]. So that we could observe the same biological samples with hard and soft x-ray fluorescence and ptychography with X-ray absorption spectroscopy in near future. We prepared HepG2 cells, a cell line derived from human hepatoma, treated with or without a newly developed antiretroviral drug, GRL-142 [4]. GRL-142 is a HIV protease inhibitor, which often showed a severe side effect of hyperlipidaemia. Therefore, we expected lipid droplets in cells treated with a high dose of GRL-142. Cells were chemically fixed with 2% paraformaldehyde in PBS and air-dried. In fact, we found increased size and number of lipid droplet-like structures in cytoplasm of the cells with GRL-142, comparing to untreated control cells, which we could hardly see the droplets by visible light microscopies without staining. Notably, we found increase the gap between nucleus and cytoplasm, and higher contrast at nucleus of the cells treated with GRL-142, which we have never seen with visible light microscopies. Higher contrast at nucleus suggested the possibility of increased the width of nucleus and/or the contents due to a stress response with a drug. It is known that cells change the width and hardness depending on the cell cycle, and chromosomes become compact against irradiation to protect them. On the other hand, we have no idea about an increased gap between nucleus and cytoplasm, although this gap may be also related to stress response by the drug. It is quite essential to figure out the molecular mechanisms of these cellular changes in near future. These changes we observed by ptychography were submitted to the article [5].

REFERENCES

[1] A. Fukunaka, et al., Scientific Report. 2023; doi: 10.1038/s41598-023-30498-y. [2] S. Matsuyama, et al., JAAS 35, 1279, 2020: doi.org/10.1039/D0JA00128G. [3] T. Kimura, et al., Opt. Express, Optics Express 30, 2022: doi: 10.1364/OE.462190. [4] H. Bulut, et al,. Scientific Report 10, 10664, 2020. [5] Y. Takeo, et al., JESRP, *under revision*.

ORBITAL CONVERSION IN COFE/CU/OXIDE

Junyeon KIM
Center for Emergent Matter Science, RIKEN

Introduction

Orbital angular moment (OAM) transport opens an emerging mechanism for the spin manipulation. Particularly, a recent experimental report presents the OAM-induced spin manipulation in CoFe/Cu/Al_2O_3 stacks is much more efficient than that by conventional mechanisms [1]. In the CoFe/Cu/Al_2O_3 stacks, nonzero OAM is polarized at the Cu/Al_2O_3 interface (Fig. 1(a)), and exerts torque when OAM is transferred to the CoFe layer. This talk is called orbital torque (Fig. 1(b)). Nowadays, the orbital torque greatly draws interest for the spin accumulation since there is no clear restrictions on materials for the nonzero OAM generation. It is apparently contrast to the spin angular momentum generation which is mainly shown in material systems consisted of heavy elements.

A recent theoretical study reports that the orbital hybridization between the *p*-orbital of oxygen atom and the *d*-orbital atom serves the formation of a chiral orbital texture by orbital Rashba effect (Fig. 1(a)) [2]. Indeed, we recently observed very large orbital torque even if we replace Al_2O_3 to other oxides such as MgO, SiO_2 and TiO_2 [3]. Particularly, orbital torque is maximum when the Oxide is SiO_2, and minium when the Oxide is Al_2O_3. For further understand on the nonzero OAM generation at the Cu/Oxide interface, we require detailed material characterization. Also observation of a modulation of the energy spectrum by a generation of nonzero OAM is also desired.

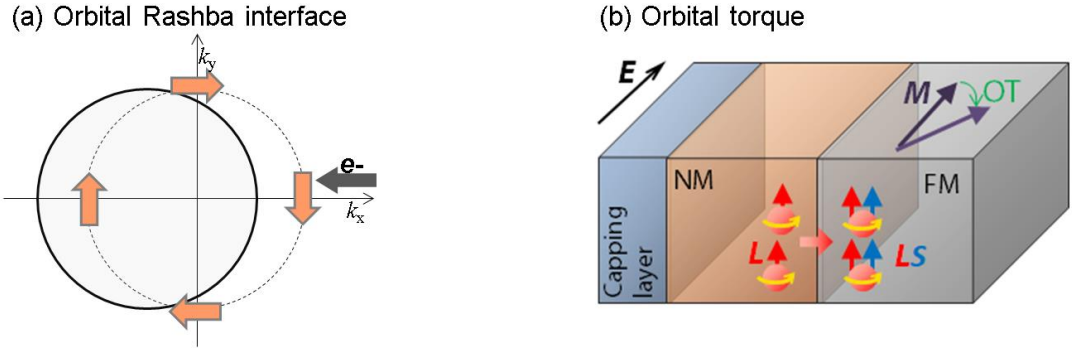

Fig. 1(a)Excess OAM generation at a chiral orbital texture. Here the chiral orbital texture is formed by orbital Rashba effect. (b) Orbital torque in FM/Cu/Oxide system.

Experimental method

For the observation of the Cu/Oxide interface, L-edge X-ray absorption spectroscopy (XAS) and X-ray magnetic circular dichroism (XMCD) was utilized. Nominally, the 3*d* orbital state of Cu is known to be fully occupied. However Grioni et al. claimed that there is still unoccupied 3*d* orbital state for Cu due to a hybridization between *s* state and *d* states [4]. And the number of unoccupied 3*d* orbital state can be promoted by formations of compounds such as CuOx. Thus we could expect the L2, 3 edge X-ray absorption.

As a first, we attempt to obtain the energy spectrum nearby the Cu/Oxide interface. Next, we also attempt to obtain a clue of the nonzero OAM generation by turning on/off the charge current.

The observation was performed in superconducting magnet magneto-optical observation system in the free board. The CoFe/Cu/Oxide stacks are electronically connected by the silver paste. And the observation was carried out by high speed switching of the circularly polarized

light and total electron yield (TEY) technique. To optimize the sample condition, 2, 5, 7, 10 nm of Al_2O_3 was tested considering with the detection length of the TEY technique (~10 nm).

Experimental results and discussion

Figure 2 displays the XAS spectra for the Al_2O_3, SiO_2, and TiO_2 samples. The XAS spectrum for the Al_2O_3 sample confirms the presence of only metallic Cu at the Cu/Al_2O_3 interface (Fig. 2(a)). On the other hand, we observe the formation of Cu oxide (CuO or Cu_2O) at the Cu/Oxide interface in the XAS spectrum for the SiO_2 (Fig. 2(b)), and TiO_2 sample (Fig. 2(c)). We speculate that the released oxygen atoms could form Cu oxides among the larger pool of released oxygen atoms. Considering the orbital torque is large in order of SiO_2, TiO_2, and Al_2O_3 capped sample, the XAS spectra support the interatomic interaction between Cu and oxygen atoms promotes the OAM polarization at the Cu/Oxide interface.

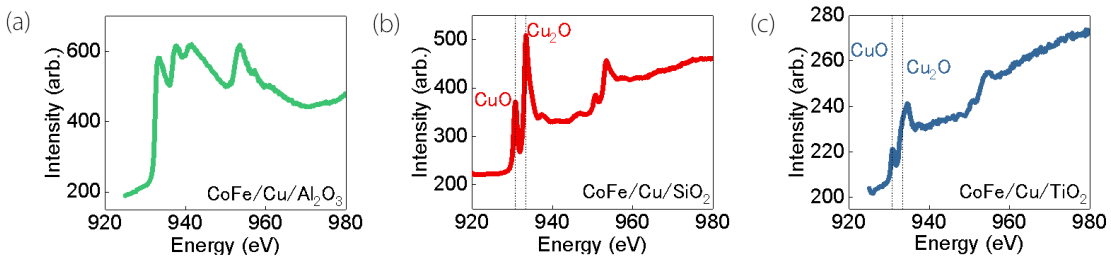

Fig. 2 (a), (b), (c) XAS spectrum for the Al_2O_3 sample (a), SiO_2 (b), and TiO_2 (c) samples. Guide lines for (b) and (c) represents the position of peak for CuO (left) and Cu_2O (right).

REFERENCES

[1] J. Kim *et al*. Phys. Rev. B **103**, L020407 (2021).
[2] D. Go *et al*., Phys. Rev. B **103**, L121113 (2021).
[3] J. Kim *et al*. Submitted to Phys. Rev. Mat.
[4]M. Grioni *et al*., Phys. Rev. B **39**, 1541 (1989).

OPERANDO X-RAY CIRCULAR DICHROISM MEASUREMENT FOR DETECTION OF ORBITAL EDELSTEIN EFFECT

Masafumi Horio[1], Tomoaki Senoo[1], Junyeon Kim[1], Yoshichika Otani[1], Iwao Matsuda[1]
[1]*The Institute for Solid State Physics, The University of Tokyo*

In order to meet the demands of the information society in recent years, increasing the performance of computing devices has become an important issue. Spintronics is a state-of-the-art technology that exploits the spin of electrons, and advances have been made in this field through research that enables high-performance manipulation of magnetism. Among these, research on spin-orbit torque (SOT) [1-3] has attracted much attention due to its scientific interest and technological applications. This technique utilizes spin transport phenomena, such as the spin Hall effect (SHE) and the Edelstein effect (EE), to inject spin into magnetic materials. These phenomena occur in systems with strong spin-orbit interaction and require heavy elements, which are rare and typically expensive. However, recent studies have reported torque generation in systems without heavy elements [4,5]. It was claimed that the experimental results can be explained by a recently proposed interfacial transport phenomenon called the orbital Edelstein effect [OEE, Fig. 1(a)]. This discovery opened the way to new techniques and increased interest in the study of spin transport phenomena at interfaces. However, no direct experimental evidence of OEE has been obtained. This is because experimental information about electronic states at interfaces has not yet been provided.

In the present study, we focused on the interface between Cu and SiO_2 where accumulation of orbital angular momentum (OAM) due to the OEE is expected [5]. We performed x-ray circular dichroism (XCD) measurements at SPring-8 BL07LSU under electric current. In order to detect accumulation of OAM, electric current was applied perpendicularly to the incident x-rays. The measurements were conducted at room temperature in the partial electron yield mode. Detailed sample structure and experimental condition are illustrated in Figs. 1(b) and 1(c), respectively.

Figure 2(a) shows Cu *L*-edge spectra under various current values. While there appear significant changes in the spectral line shape, the influence of electric current cannot be separated from gradual temporal changes confirmed by performing measurements repeatedly in the same condition [Fig. 2(b)]. The "contamination" from this temporal change by x-ray irradiation is inevitable if one makes a full energy scan across the Cu *L*-edge, which takes ~30 minutes. In order to extract genuine effects of current application, we fixed the photon energy at 934.5 eV and monitored absorption intensity for a short time (~several minutes) while repeatedly turning on and off electric current. Figures 2(c) and 2(d) show the results of such measurements performed with left and right circular polarization (LCP and RCP). In both measurements, decrease of absorption intensity was observed due to the generation of

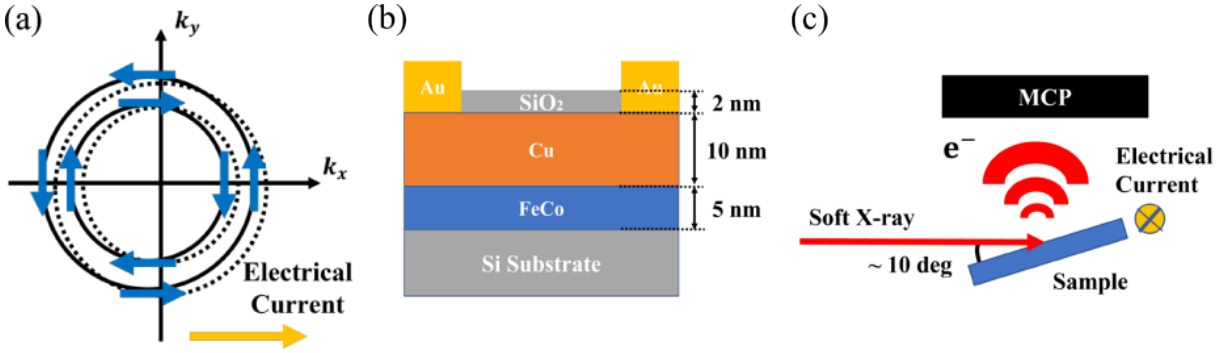

Fig. 1: Experimental setups. (a) Schematic illustration of OEE. (b) Sample structure. (c) Geometry of XCD measurements.

magnetic field that traps electrons and moves them back to the sample. Comparing the magnitude of the intensity decrease between the measurements conducted with right and left circular polarization, we found larger decrease for RCP. According to the sum rule of x-ray magnetic circular dichroism, this is consistent with expectation from OEE shown in Fig. 1(a) Utilization of fast polarization switching that has been developed at SPring-8 BL07LSU [6] may pave the way for further clarifying the effect of electric current and eventually proving the occurrence of OEE.

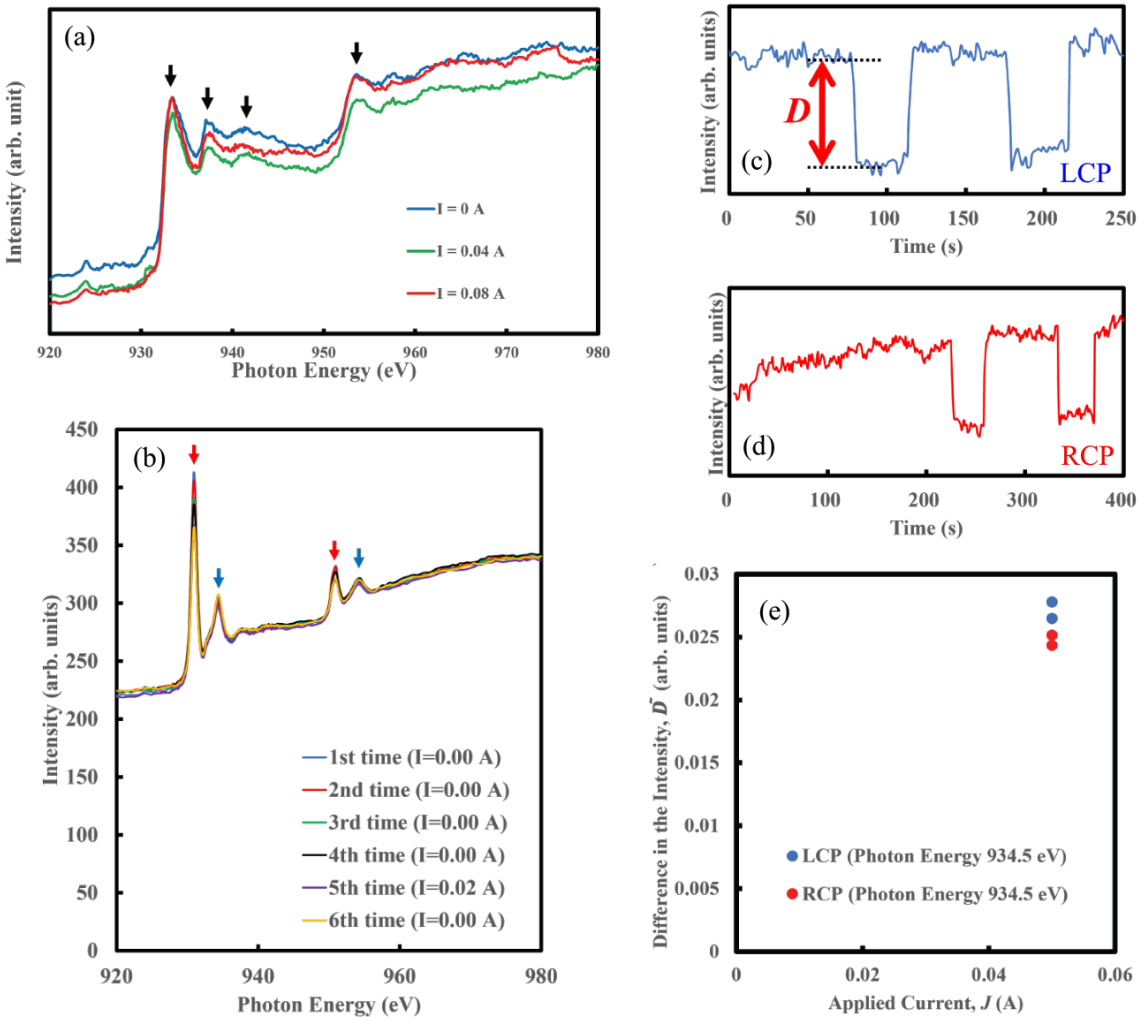

Fig. 2: XCD results on the Cu/SiO_2 sample. (a) Cu *L*-edge spectra measured under electric current as indicated. (b) Cu *L*-edge spectra measured repeatedly. (c),(d) Absorption intensity as a function of time measured at the photon energy of 934.5 eV with LCP and RCP. Sharp decrease is observed upon application of electric current. (e) Magnitude of intensity decrease for LCP and RCP.

REFERENCES

[1] I. M. Miron *et al*., Nature **476**, 189 (2011).
[2] L. Liu *et al*., Science **336**, 555 (2012).
[3] A. Manchon *et al*., Rev. Mod. Phys. **91**, 035004 (2019).
[4] H. An *et al*., Nat. Commun. **7**, 13069 (2016).
[5] J. Kim *et al*., Phys. Rev. B **103**, L020407 (2021).
[6] J. Miyawaki *et al*., AAPPS Bulletin **31**, 1-24 (2021).

XPS ANALYSES OF THE NOVEL SURFACE PHASES, GROWN BY BORON DEPOSITION ON A COPPER CRYSTAL SURFACE

Yuki Tsujikawa, Xiaoni Zhang, Masafumi Horio, Tetsuya Wada, Masashige Miyamoto, Toshihide Sumi, Fumio Komori, Iwao Matsuda
Institute for Solid State Physics, The University of Tokyo

Takahiro Kondo
Department of Materials Science and Tsukuba Research Center for Energy Materials Science, Faculty of Pure and Applied Sciences and R&D Center for Zero CO_2 Emission with Functional Materials, University of Tsukuba

In a history of surface science, a numerous number of the ordered phases were observed at various crystal surfaces, depending on adsorbate elements, coverages, or growth conditions. Recently, there have been growing interests in chemistry and physics of boron polymorphs or metal borides on surfaces due to unique multi-center bonding between boron atoms [1]. On the well-known Cu(111) substrate, the 2D ordered phase, $\sqrt{73}\times\sqrt{39}$, is prepared by boron deposition [2]. Structure analysis by the diffraction method unveiled that a 2D Cu-B compound, Cu boride is formed at the surface [3]. On the other hand, by the boron deposition on Cu(110), we discovered a 1D anisotropic ordered phase, 3×1, as a pattern of electron diffraction [4]. These novel B/Cu surface phases are intriguing playgrounds to explore the electronic or chemical states of these elements at the interface. In the present research, we conducted experiments of high-resolution X-ray photoelectron spectroscopy to confirm the electronic structure of these B/Cu .

The XPS measurement was made at the soft X-ray beamline BL07LSU of the synchrotron radiation facility SPring-8 with the electron analyzer (Phoibos-150 NAP, Specs Co.). All the data were obtained at room temperature. A sample was prepared on the surface of commercial crystals of Cu(110) and Cu(111). The surface phases was prepared by boron deposition on a clean surface of Cu(110) or Cu(111). The ordered structures were examined by observations of low energy electron diffraction (LEED), while the chemical states were investigated by XPS. As shown in Fig.1, only signals of B and Cu were observed, confirming no detectable impurity.

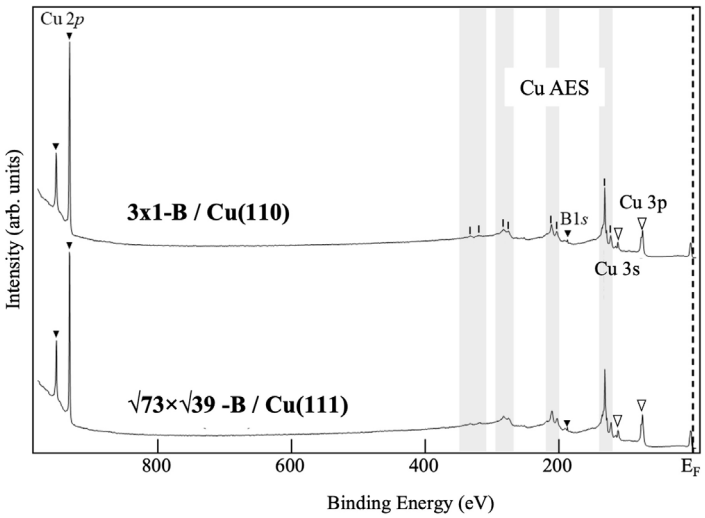

Figure 1 XPS spectra of the ordered surface phases of B/Cu(110) and B/Cu(111), taken at photon energy of hν = 1050 eV. Peaks of the B and Cu core-levels are indicated with black and white arrows, respectively. Signals of Auger electron spectroscopy (AES) are shown for Cu by gray bars.

Figure 2 shows XPS spectra of the Cu $2p_{3/2}$ and B 1s core level of the $\sqrt{73}\times\sqrt{39}$-B/Cu(111) surface. The sample has two Cu components of the surface layer (L) and in the bulk (Bu), while a clean Cu(111) surface is composed of a single component besides the negligible defect remanent. The (L) component can be identify as the surface Cu atom in Cu boride. In contrast, the B 1s spectrum of the $\sqrt{73}\times\sqrt{39}$-B/Cu(111) surface has a single component. The binding energy of 187.8 eV, determined from curve fitting, indicates that the boron atoms are

negatively charged [3]. It is likely that electrons were transferred to the boron atoms from the surrounding copper.

The surface phase of the 3×1-B/Cu(110) was discovered by us at the SPring-8 beamline, BL07LSU, by LEED [4]. The XPS spectrum of the Cu $2p_{3/2}$ core-level, as measured *in situ*, is curve-fitted with two components, as shown in Fig.3. In addition to the peak (Bu), ascribed to the clean Cu(110) surface, a new component, labelled (L), can be found. Since the Cu atom in the bulk crystal (Bu) has neutral charge, the peak position of the L component at the higher binding energy indicates that the Cu atoms in the 2D phase are positively charged. On the other hand, the B 1*s* core-level spectrum can be curve-fitted by two components, labelled I and II. The major component (I) is naturally assigned to the 3 × 1-B/Cu(110) surface, while the minor component (II) can be ascribed to either a part of the surface phase or the other contributions, such as surface impurities. By a comparison with Fig.2, binding energy of the component (I) at 187.4 eV indicates that the boron atoms in the 3 × 1-B phase are also negatively charged. The similarity with √73×√39-B/Cu(111) result suggest that the 3 × 1-B/Cu(110) phase are also a 2D Cu-B compound.

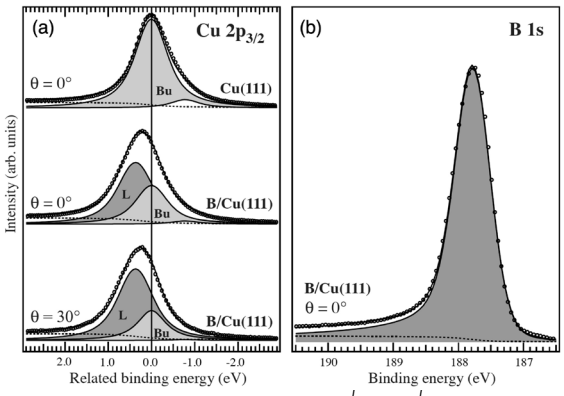

Fig.2 XPS spectra of the √73×√39-B surface phase on Cu(111): (a) Cu $2p_{3/2}$ and (b) B 1*s* core-level. Photon energies were (a) hν = 1050 eV and (b) hν = 285 eV. For a reference, a spectrum of the clean Cu(111) surface is shown. The peak components are obtained by the curve-fits and labeled with different symbols.

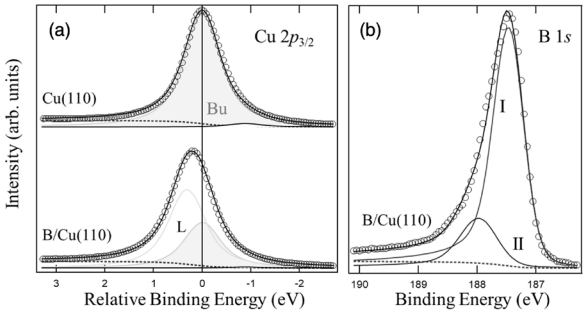

Fig.3 XPS spectra of the 3×1-B surface phase on Cu(110): (a) Cu $2p_{3/2}$ and (b) B 1*s* core-level. Photon energies were (a) hν = 1050 eV and (b) hν = 285 eV. For a reference, a spectrum of the clean Cu(110) surface is shown. The peak components are obtained by the curve-fits and labeled with different symbols.

In conclusion, we found that the boron atoms were negatively charged in the surface phases of √73×√39-B/Cu(111) and 3×1-B/Cu(110). The unique electronic property has also been known in the previous research of 2D boron or borophene [1]. The layer itself is unstable in the free-standing form but stable on a 2D metal substrate after electron doping. These microscopic findings indicate that low-dimensional boron structures on surfaces likely have the universal electrophilic property.

REFERENCES

[1] I. Matsuda, K. Wu ed., 2D Boron: Boraphene,Borophene, Boronene (Springer, 2021).
[2] R. Wu, I. K. Drozdov, S. Eltinge, P. Zahl, S. Ismall-Belgl, I. Božović, and A. Gozar, Nat. Nanotech. **14**, 44 (2019).
[3] Y. Tsujikawa, M. Horio, X. Zhang, T. Senoo, T. Nakashima, Y. Ando, T. Ozaki, I. Mochizuki, K. Wada, T. Hyodo, T. Iimori, F. Komori, T. Kondo, I. Matsuda, Phys. Rev. B **106**, 205406 (2022).
[4] Y. Tsujikawa, X. Zhang, M. Horio, T. Wada, M. Miyamoto, T. Sumi, F. Komori, T. Kondo, I. Matsuda, Surf. Sci. **732**, 122282 (2023).

ELECTRONIC STRUCTURE OF WATER CONFINED IN AQUEOUS MICROPHASE TWO-PHASE SYSTEMS

Yuji Higaki, Takumi Masuda
Faculty of Science and Technology, Oita University

Introduction

A large number of studies for the irregular structure and dynamics of water confined in nanometer scale molecular assembly including reverse micelles, and recently, metal-organic frameworks, carbon nanotubes, and polymer brushes.[1,2] Water molecules involved in hydration of ions experience constraints which prevent the formation of the preferred tetrahedral configurations characteristic of bulk water to cause hydrogen-bonding distortion. The hydrogen-bonding state of water has been studied by spectroscopic methods such as infrared spectroscopy, sum frequency generation spectroscopy, and solid-state NMR measurements. Soft X-ray absorption (XAS) and soft X-ray emission (XES) spectroscopies have recently attracted attention for their ability to show the detailed hydrogen bonding configurations from the electronic structures of the oxygen responsible for the hydrogen bonds.[3]

We developed a new class aqueous phase separation system of double hydrophilic block copolymers.[4] Double hydrophilic block copolymers comprising two kinds of zwitterionic polymers, poly(carboxybetaine methacrylate) (PCB2) and poly(sulfobetaine methacrylate) (PSB4), exhibits microphase separation in the highly concentrated aqueous solution to produce a highly ordered periodic lattice structure with nanometre scale compartments, and the morphology transforms in response to the polymer concentration (**Figure 1**). This morphology transition is manifested by selective water partitioning to the PCB2 phase owing to the poor water capacity of PSB4 phase. The double hydrophilic microphase-separated structure involving hydration water could be a good prototype for investigating the structure and dynamics of water confined in the fields with crowded charged polymers.

In this study, hydrogen bonding configurations of waters confined in the microphase separated zwitterionic mesophases were investigated by meas of XAS and XES spectroscopies. Systematic experiments were conducted by adjusting the polymer concentration in the microphase-separated structure to address the impact of microphase separation at the electronic structure level and to elucidate detailed information on the hydrogen bonding form and its role in microphase separation.

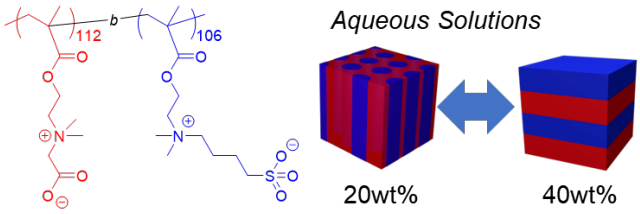

Figure 1. Chemical structure of the PCB2$_{112}$-*b*-PSB4$_{106}$ block copolymer and the schematic of morphologies.

Experiment

PCB2$_{112}$ (M_n = 24400, M_w/M_n = 1.12), PSB4$_{102}$ (M_n = 30200, M_w/M_n = 1.10), and the diblock copolymer PCB2$_{112}$-*b*-PSB4$_{106}$ (M_n = 54000, M_w/M_n = 1.19, , volume fraction of PCB2 = 0.41) were synthesized by reversible addition fragmentation chain transfer polymerization. The molecular mass and molecular mass distribution were well-controlled. The PCB2$_{112}$-*b*-PSB4$_{106}$ diblock copolymer aqueous solution produces microphase separated structure with lamellar morphology, where the long period was 46.2 nm and the PCB2 lamellar thickness was 28.0 nm, at polymer concentration (ϕ) = 40wt%, while the morphology transforms to columnar morphology with hexagonally packed cylindrical domains, where the cylinder radius is 13.2 nm and the cylinder center distance is 52 nm at ϕ = 20wt%.

XES and XAS measurements were conducted at the BL07LSU HORNET station at Spring-8 employing home-made liquid cell (**Figure 2**). The aqueous solution of PCB2-*b*-PSB4 diblock

copolymers were put onto the SiC membrane separating vacuum chamber, and the cell was sealed with a screw cap. Milli-Q water (Millipore Inc., Billerica, MA) with a resistance of >18 MΩ cm was used as the water source. The excitation energy was 550 eV, which is well above the ionization threshold. Each XES spectrum was normalized with the integration of the intensity between 515 and 530 eV to compare the spectrum shape.

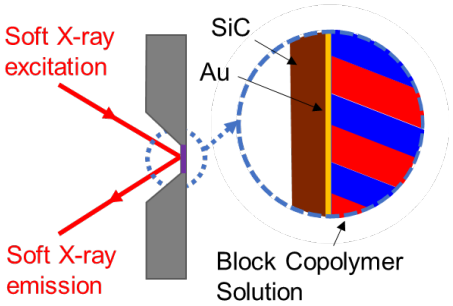

Figure 2. Schematic representation of the experimental setup for the XES spectroscopy of water confined in the microphase separated PCB2$_{112}$-*b*-PSB4$_{106}$ aqueous solutions.

Results and Discussion

The hydrogen-bonding structure configurations of water confined in microphases were investigated by O 1s XES spectroscopy. XES spectra of the PCB2$_{112}$-*b*-PSB4$_{106}$ aqueous solutions exhibited two peaks at 525.8 eV and 526.7 eV, which have been assigned to the oxygen of water with distorted and tetrahedral hydrogen bonding configurations, respectively (**Figure 3(a)**).[4] In comparison with the XES spectrum of bulk water, the 1b$_1$" peak intensity was pronounced with respect to 1b$_1$' peak, indicating the significant hydrogen-bonding distortion in the water confined in the zwitterionic polymer mesophase. Meanwhile, the XES spectrum shape was independent of the ϕ. This result suggests that the hydrogen bonding distortion remains identical with decreasing the zwitterionic PCB2$_{112}$-*b*-PSB4$_{106}$ concentrations. Since the PSB4 phase has water capacity limit at approximately 50wt%, the PCB2 phase contains relatively more water and its polymer concentration can be estimated to 32.2, 20.2, and 11.6wt% when the block copolymer concentrations are 40, 30, 20wt%, respectively. Thus, the hydrogen-bonding state of water in the mesoscopic phase-separated structures of lamellar structure with 50wt% PSB4 and 32.2wt% PCB2 phases, and the columnar structure with 50wt% PSB4 cylindrical domains and 11.6wt% PCB2 matrix were identically distorted.

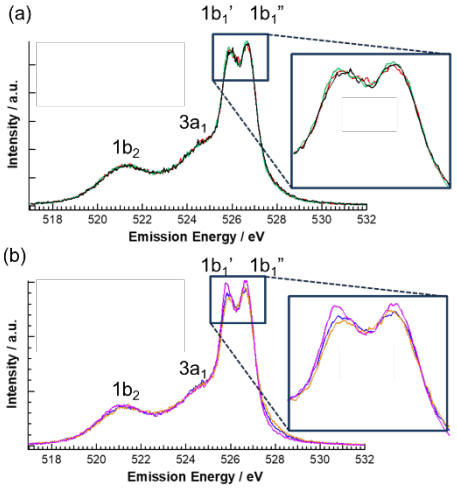

Figure 3. XES spectrum of (a) PCB2$_{112}$-*b*-PSB4$_{106}$ aqueous solutions with ϕ = 40wt% (black), 30wt% (red), and 20wt% (blue), and (b) PCB2$_{112}$ aqueous solutions with ϕ = 40wt% (yellow) and 10wt% (purple), and a PSB4$_{102}$ aqueous solution with ϕ = 40wt% (blue). The additional panels show magnified data at 1b$_1$' and 1b$_1$" peaks.

We then verified the hydrogen bonding configuration of water in PCB2 and PSB4 solutions (**Figure 3(b)**). The 40wt% PCB2 and 40wt% PSB4 aqueous solutions showed the XES spectra comparable to PCB2$_{112}$-*b*-PSB4$_{106}$ solutions. On the other hand, the 10wt% PCB2 solutions showed a slight increase in the intensity of 1b' peak relative to the 1b", while the spectrum is identical to that of bulk water. Thus, the water molecules in the PCB2 phase of the microphase separated 20wt% PCB2$_{112}$-*b*-PSB4$_{106}$ solution are perturbed relative to those in PCB2 solutions, probably because of the obstruction of hydrogen bonding network due to the phase boundary.

REFERENCES

[1] M. A. Wells, *Biochemistry* **1974**, *13*, 4937–4942.

[2] K. Yamazoe, Y. Higaki, Y. Inutsuka, J. Miyawaki, A. Takahara, Y. Harada, *Langmuir* **2022**, *38*, 3076.

[3] T. Tokushima, Y. Harada, O. Takahashi, Y. Senba, H. Ohashi, L. G. M. Pettersson, A. Nilsson, S. Shin, *Chem. Phys. Lett.* **2008**, *460*, 387.

[4] Y. Higaki, M. Takahashi, T. Masuda, *Macromol. Chem. Phys.* **2022**, *224*, 2200416.

SOFT X-RAY EMISSION SPECTROSCOPIC ANALYSIS OF 1D WATER CHANNEL WITHIN A NONCOVALENT POROUS CRYSTAL

Shinnosuke HORIUCHI,[1,2] Shota OGURA,[1] Yuka IKEMOTO,[3] Hisao KIUCHI,[4] Kazuo TATSUTA,[4] Yusuke TOMIYORI,[4] Yoshihisa HARADA[4]

[1]*Division of Chemistry and Materials Science, Graduate School of Engineering, Nagasaki University*

[2]*Department of Basic Science, Graduate School of Arts and Sciences, The University of Tokyo*

[3]*Spectroscopy Division, Japan Synchrotron Radiation Research Institute*

[4]*Synchrotron Radiation Laboratory, The Institute for Solid State Physics, The University of Tokyo*

Water molecules on material interfaces play crucial roles in abundant natural phenomena and material sciences [1,2]. Although the importance of interfacial water has been recognized, it is still challenging to elucidate a three-dimensional alignment of water clusters and the hydrogen-bonding network on a non-flat material surface in an atomic resolution. Recently, X-ray diffraction studies using crystalline porous materials can visualize not only the absolute configuration of small molecules but clustering motifs of the guests on the pore surface [3–5]. In addition, X-ray emission spectroscopy (XES) is one of the useful techniques to probe electronic transitions between core and valence orbitals of oxygen atoms, which can provide useful information reflected from the hydrogen-bonding states of water molecules, because the time scale of the excitation process and the O1s core-hole lifetime in femtoseconds are much shorter than that related to rearrangements of the hydrogen-bonding network [6]. Thus, the combination of these techniques will provide a clear relationship between a structure and its character of a water cluster formed on the pore surface of the crystalline material.

We have recently synthesized a supramolecular crystal composed of coordination complex salts and macrocyclic organic hosts (Figure 1). The supramolecular crystal contained one-dimensional (1D) water channels in the crystal lattice, where the molecular alignments of the water molecules can be determined by the single crystal X-ray diffraction analysis. In particular, the large water cluster and its temperature-dependent dynamic character were observed in the X-ray analysis. This result suggests that this supramolecular crystal containing 1D water channels is a suitable material for elucidating the inhomogeneous nature of interfacial water molecules. Thus, for unveiling the electronic structure of the water molecules in the 1D pore, we performed the soft X-ray emission spectroscopic analysis of the 1D water channels within the supramolecular crystal.

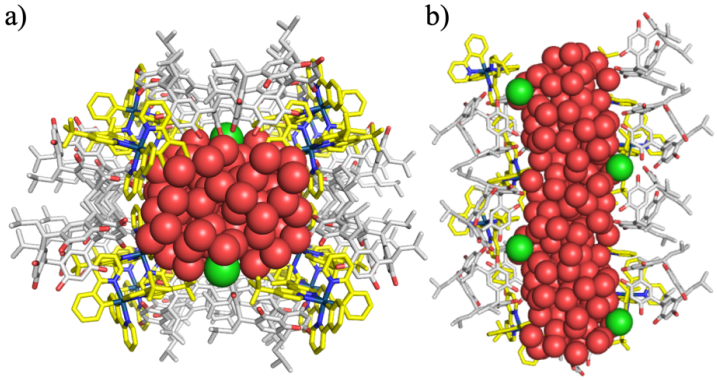

Figure 1. Crystal structures of the supramolecular crystal viewed from a) the top and b) the side of the 1D water channels. Red spheres represent oxygen atoms of the water molecules in the pore.

The supramolecular crystal contains hydroxy (–OH) groups in the framework. Thus, the dehydration process of the crystal was investigated by the O1s XES measurement to eliminate the effect of the framework. The XES measurement was performed using the SPring-8 BL07LSU ultra-high resolution soft X-ray emission spectrometer HORNET. During the measurement, a steam-nitrogen gas mixture flowed over the sample, enabling precise control of humidity around the sample and the dehydration rate. The intensities of the XES spectra during the dehydration process were summarized in Figure 2a. The intensity of the spectra

gradually decreased and was mostly constant after 400 min. This result indicates that the dehydration process was completed at 400 min and the spectra after 400 min are derived from the hydroxy groups in the framework. Thus, the XES spectra of the water molecules in the 1D pore of the supramolecular crystal were obtained from the difference spectra using the averaged spectra recorded from 600 to 745 min as a background spectrum. As a result, the difference spectrum showed characteristic features of water molecules, which involved four peaks assigned to $1b_1$", $1b_1$', $3a_1$, and $1b_2$, respectively (Figure 2b). In general, the XES spectrum of bulk liquid water consists of the four peaks corresponding to oxygen 2p orbitals of water, which are obtained by the emitted X-ray associated with the electronic transition from the valence state to the core level. These spectral features can be associated with two distinct structural motifs in liquid water, where the $1b_1$' peak at 525.8 eV and the $1b_1$" peak at 526.7 eV correspond to fourfold icelike hydrogen-bonds and less than fourfold highly distorted hydrogen-bonds, respectively (Figure 2c). The relative intensities of the two $1b_1$ peaks are dependent on the measurement conditions, which will provide spectroscopic aspects for the hydrogen bonding of water molecules in the 1D pore. Intriguingly, the intensity of $1b_1$" at 526.7 eV was higher than that of $1b_1$' at 525.8 eV. This result strongly suggests that the structure of water molecules in the 1D pore is mainly less than fourfold highly distorted hydrogen-bonds even at ambient conditions, rather than fourfold icelike hydrogen-bonds. Variable-temperature X-ray diffraction studies revealed that the water molecules in the 1D pore showed temperature-sensitive and dynamic characteristics. Thus, these XES results clearly explained the flexible character of the hydrogen-bonding network of the water molecules in the supramolecular crystal.

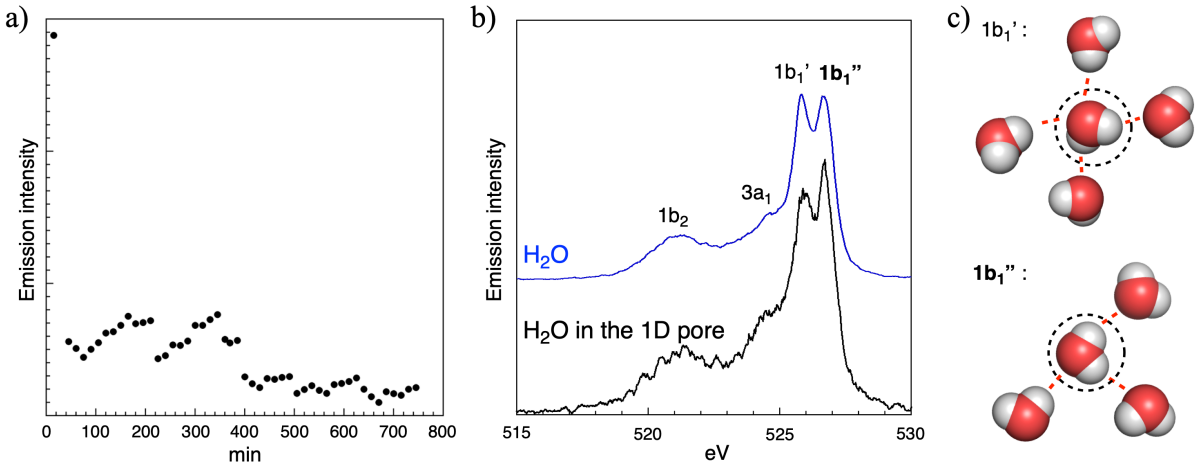

Figure 2. a) Emission intensities of the XES spectra. b) The O1s X-ray emission spectra of bulk liquid water (blue line) and H_2O molecules in the 1D pore (black line). c) Molecular structures of fourfold icelike hydrogen-bonds (upper) and less than fourfold highly distorted hydrogen-bonds (bottom) of water molecules.

In summary, O1s XES spectra of water molecules in the supramolecular crystal were obtained by following the dehydration process of the crystal. The XES spectra indicated that the crystal contained weakly hydrogen-bonded waters in the 1D channel, which is well-reflected with the dynamic character of water molecules observed in the X-ray crystallographic study. This combination study provides a clear relationship between the hydrogen-bonded structure and temperature-sensitive and dynamic characteristics of the interfacial water molecules.

REFERENCES

[1] Björneholm, O. et al. *Chem. Rev.* **116**, 7698 (2016).
[2] Brini, E. et al. *Chem. Rev.* **117**, 12385 (2017).
[3] Inokuma, Y. et al. *Nature* **495**, 461 (2013).
[4] R. Kubota, *Nat. Chem* **6**, 913 (2014).
[5] Hanikel, N. et al. *Science* **374**, 454 (2021).
[6] Fransson, T. et al. *Chem. Rev.* **116**, 7551 (2016).

Electronic states analysis of oxygen evolution reaction catalyst for alkaline water electrolysis by Operando soft X-ray absorption/emission spectroscopy

Kazuo Tatsuta[a*], Jun Kikuma[b], Shinya Matsuno[b], Shin Kawashima[b], Hisao Kiuchi[a], and Yoshihisa Harada[a]
[a]The Institute for Solid State Physics, the University of Tokyo, [b]Asahi Kasei Corporation
*Current affiliation: Asahi Kasei Corporation

In improving the efficiency of hydrogen generation by water electrolysis, there are two important factors: one is to reduce the voltage above the theoretical electrolysis voltage that must be applied for the electrolytic reaction (overvoltage), and the other is to suppress the increase in overvoltage due to catalyst degradation. Various electrocatalysts have been developed to solve these problems. Perovskite-type oxides acting as anode catalysts have a wide range of elemental choices, among them, $LaNiO_3$ is particularly promising in the next-generation alkaline water electrolysis system because of its high electrical conductivity and stable oxygen evolution reaction (OER) in the alkaline electrolyte. Our previous studies have confirmed that the addition of a small amount of transition metal elements to $LaNiO_3$ can suppress catalyst degradation for a long time, however little difference was found by hard X-ray absorption spectroscopy (XAS) of Ni, and the correlation between durability during operation and the chemical stability of Ni could not be found. On the other hand, the use of soft X-ray emission spectroscopy (XES), which can directly observe the strength of orbital hybridization and charge transfer energy expected to clarify the correlation between durability and the chemical state of Ni. Therefore, in this study, we worked on the development of a technique to perform Ni-L edge XES measurements of $LaNiO_3$ under alkaline water electrolysis operando conditions, with the aim of providing feedback for further anode material optimization.

The cell for Operando measurement was based on the liquid cell developed by Tokushima et al.[1], and was modified to enable water electrolysis in a three-electrode system by inserting contact probes for the reference electrode (RE), counter electrode (CE), and working electrode (WE). A screw-in Ag/AgCl RE was screwed directly into the cell. A 0.5 mm diameter Pt wire was used as CE, inserted into the electrolyte channel in the cell, and the insertion opening was sealed with epoxy resin. The membrane with 150 nm thick Si_3N_4 window with $LaNiO_3$ and Au/Ti layers was used as WE. The cell was fabricated with acrylic resin using a 3D printer. A 20% KOH solution was used as the electrolyte, and the flow rate was 10 ml/min during Operand measurement.

All measurements described below were performed on the beamline BL07LSU at SPring-8. Before Operando measurement, ex-situ Ni-L edge XAS and XES measurements were carried out on $LaNiO_3$ surface. The samples for Operando measurement were previously energized at 0.55 V, which is the OER potential, for 6 hours to confirm that the OER activity was enhanced. Before XES measurements, XAS measurements were performed. For Operando Ni-L edge XAS measurements, applied potentials were 0.35 V (before OER), 0.57 V (during OER), and the open circuit potential, and performed at several different points on the Si_3N_4 window to prevent damage to the window by X-rays. For Operando Ni-L edge XES measurements, the excitation energies were set to 853.2 eV. To prevent damage to the Si_3N_4 window caused by X-ray irradiation, the irradiation positions were changed every 2 min, and the data were obtained by integrating the spectra from all measurement positions. The applied potentials were 0.35 V and 0.57 V.

The obtained XAS spectra were normalized to the peak intensity at 853 eV for the operando measurement results, and the spectra obtained at multiple measurement positions were

arranged by measurement potential and are shown in Figure 1 together with the ex-situ measurement results. The peak at 850.6 eV is an absorption peak of La-M_4. The spectral shape obtained by ex-situ measurement was similar to that of $LaNiO_3$ deposited by laser deposition[2]. On the other hand, most of the spectral shapes obtained by the operando measurement were significantly different from those by the ex-situ measurement, and the shapes differed depending on the measurement positions. The spectral shapes obtained from the operando measurements, characterized by a peak on the high energy side (~855eV) of Ni-L_3 that is significantly lower than the peak on the low energy side (~853eV), suggest that the catalyst layer exists as a compound with predominantly Ni^{2+} components[3]. This result suggests that the catalyst layer has already changed to a chemical state different from that of $LaNiO_3$ during pre-energization. The large variations in spectral shape from position to position did not allow us to determine the spectral change with potential.

The obtained XES spectra are shown in Figure 2 together with the results of ex-situ measurement, normalized by the intensity of the main peak, where the abscissa axis is represented as energy transfer. The Operando measurements were integrated for about 5 hours, but because the noise was very high in all cases, no characteristic structures other than the main peak around 1 eV could be identified, and the structural differences between the spectra were also unclear, making it impossible to clarify changes due to electric potential.

In order to elucidate the cause of the variation of XAS spectra by measurement positions and the large noise in XES spectra, cross-sectional SEM and TEM observations of the catalyst layer on the Si_3N_4 window of the samples used for operando measurements were performed and thickness variation of about 5 nm to 300 nm was observed. It is suggested that the variation in thickness correlates with the variation in the chemical state of the catalyst layer and is the cause of the variation in the shape of the XAS spectra. In addition, there are many thin regions, which may have resulted in insufficient intensity and increased noise in XES spectra, in which the emission intensity was integrated by scanning over the window. These results clearly indicate that improving the thickness uniformity of $LaNiO_3$ on the Si_3N_4 window is a future challenge.

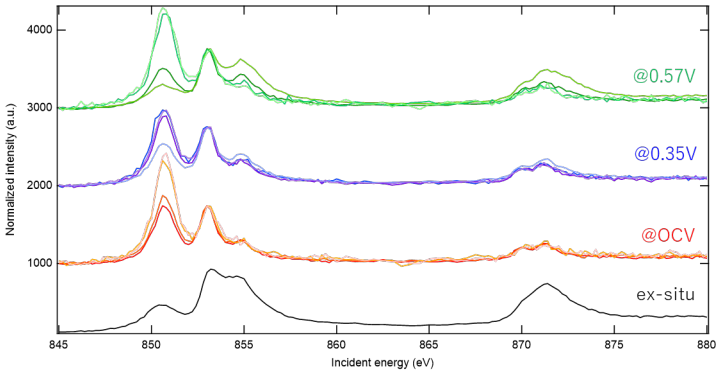

Fig.1 ex-situ and Operando Ni-L edge XAS spectra

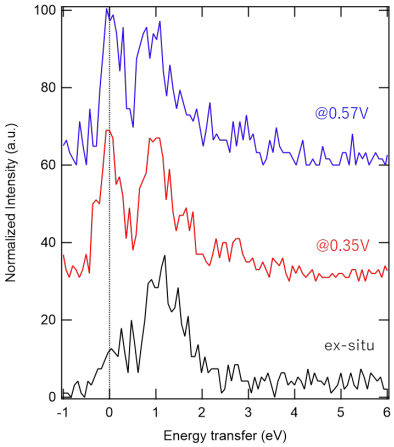

Fig.2 ex-situ and Operando Ni-L_3 edge XES spectra obtained at excitation energy of 853.2 eV

REFERENCES

[1] T. Tokushima, Y. Harada, Y. Horikawa, O. Takahashi, Y. Senba, H. Ohashi, L. G. M. Pettersson, A. Nilsson, S. Shin, *J. Electron Spectrosc. Relat. Phenom.*, 177 (2010) 192.
[2] M. Hepting, D. Li, C. J. Jia, H. Lu, E. Paris, et al., *Nat. Mater.*, 19 (2020) 381.
[3] C. Tian, D. Nordlund, H. L. Xian, Y. Xu, Y. Liu, D. Sokaras, F. Lin, and M. M. Doeff, *J. Electrochem. Soc.*, 3 (2018) A696

ELECTRONIC STRUCTURE ANALYSIS OF OXYFLUORIDE CATHODE OF ALL-SOLID-STATE FLUORIDE BATTERY USING RESONANT INELASTIC X-RAY SCATTERING

Kentaro YAMAMOTO[1,2], Datong ZHANG[1], Hisao KIUCHI[3], Yoshihisa HARADA[3], Yoshiharu UCHIMOTO[1]

[1]*Graduate School of Human and Environmental Studies, Kyoto University*

[2]*Faculty of Engineering, Nara Women's University, Kitauoyanishimachi, Nara, 630-8263*

[3]*Synchrotron Radiation Laboratory, The Institute for Solid State Physics, The University of Tokyo*

All-solid-state fluoride-ion rechargeable batteries are expected to be high-power, high-energy density rechargeable batteries because they can use multi-electron transfer reactions with monovalent fluoride-ions as carriers. Until now, development of cathode materials has focused on simple metal/metal fluoride (M/MFx) systems[1,2]. However, the absence of a diffusion path for F^- during the fluorination and defluorination reactions and the large volume change associated with the fluorination and defluorination reactions of the most densely packed metal cathodes (such as Cu) have made it difficult to achieve the following rate characteristics. In this study, we focused on Cu_3N as a new cathode material to solve this problem, because Cu_3N cathode has many anion vacancy sites in its structure and is expected to show better rate characteristics than metal cathodes. The reaction mechanism was further elucidated by electron spectroscopy.

Cu_3N was synthesized by mixing Cu_2O and $CO(NH_2)_2$ in the ratio of 1:2 mol, annealing at 190°C for 6 h, and washing and drying[3]. A bulk-type electrochemical cell was constructed with $Cu_3N/La_{0.9}Ba_{0.1}F_{2.9}$/Vapor grown carbon fiber (VGCF) as a composite positive electrode, $La_{0.9}Ba_{0.1}F_{2.9}$ as an electrolyte and $Pb/PbF_2/La_{0.9}Ba_{0.1}F_{2.9}$/VGCF as a composite negative electrode. Charge-discharge measurements were performed in the cutoff voltage range of -1.5 to 2.9 V at 140°C. Cu K, *L*-edge XAS and N *K*-edge XAS, RIXS measurements were performed on the samples after charge and discharge.

The charge-discharge curve measurements of the Cu_3N cathode are shown in Figure 1. The Cu_3N cathode exhibits reversible charge-discharge behavior within the Cu^+/Cu^{2+} redox range, while showing a potential flat area at about 0.65 V (vs. Pb/PbF_2) (Figure 1 a). Charge and discharge capacities of 290 mAh g^{-1} and 236 mAh g^{-1} were obtained during initial charge and discharge, respectively. The Cu_3N cathode maintained a charge and discharge capacity of 100 mAh g^{-1} even when the current density was increased to 200 mA g^{-1}, showing higher rate and cycle properties than the Cu cathode. Furthermore, the Cu_3N cathode showed an extremely high capacity of 780 mAh g^{-1} on initial charge and 550 mAh g^{-1} on discharge, exceeding the theoretical capacity (393 mAh g^{-1}) of the Cu^+/Cu^{2+} redox (Figure 1b).

Cu *L*-edge, N *K*-edge XAS and RIXS measurements were performed on Cu_3N during the charging process to clarify the origin of this capacitance that cannot be explained by the Cu^+/Cu^{2+} redox. In the Cu *L*-edge XAS spectra, a peak was observed at about 930.5 eV; toward F=3, this peak shifted to the lower energy side with charging, and the peak position of the sample charged up to F=3 was consistent with that of CuF_2. Subsequently, when the samples were charged from F=3 to F=6, no change in peak position was observed. These results indicate that oxidation of Cu^+ to Cu^{2+} occurred from F=0(pristine) to F=3, but that Cu was not oxidized from F=3 to F=6. In the N *K*-edge XAS spectra (Figure 2a), no noticeable change in spectral shape with charging was observed from F=0(pristine) to F=2. On the other hand, from F=2 to F=6, the peak shape around 401 eV changed and the peak intensity increased dramatically. This dramatically changed peak shape is very similar to that of nitrogen gas[4]. In the N *K*-edge RIXS spectrum at 400.8 eV, vibrations similar to those of N_2 gas in the previous study[5], and the value

of the width of the Cu_3N frequency is consistent with the N_2 gas value (2360 cm^{-1}, 0.292 eV), suggesting the presence of N_2 molecules within Cu_3N. These results indicate that nitrogen redox occurs in the Cu_3N cathode during charging, leading to the high capacity.

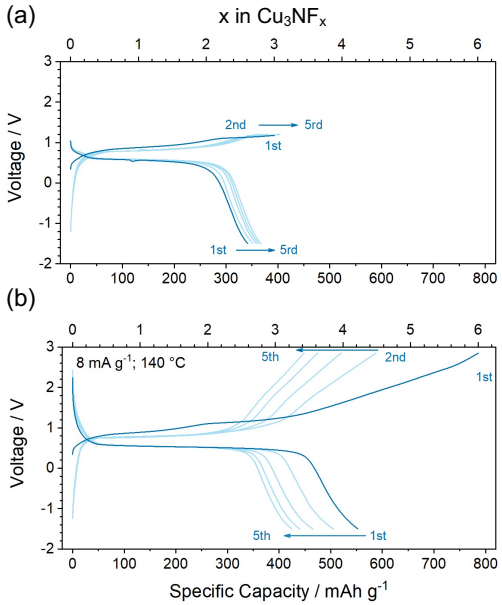

Fig. 1. Electrochemical measurements of Cu_3N cathode material at 140 °C. Charge/discharge profiles under capacity limitation of (a) F=3 and (b) F = 6 at 8 mA g^{-1}.

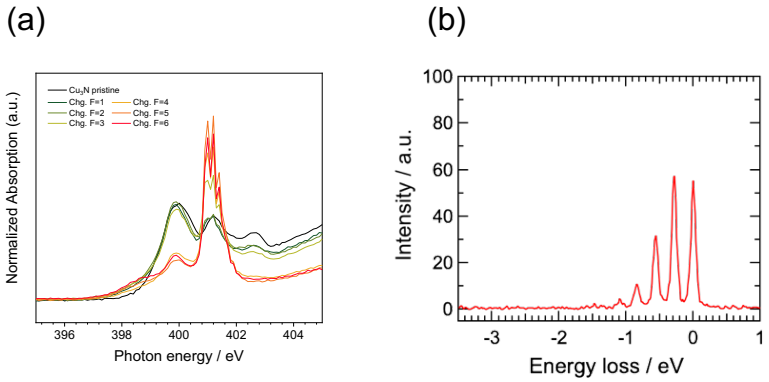

Fig. 2. (a) N *K*-edge XANES spectra of Cu_3N cathode obtained upon charging and (b) N *K*-edge RIXS spectrum of Cu_3N cathode after full charging.

REFERENCES

[1] M. Anji Reddy and M. Fichtner, *J. Mater. Chem.* 2011, **21**, 17059–17062.

[2] D. Zhang, K. Yamamoto, A. Ochi, Y. Wang, T. Yoshinari, K. Nakanishi, H. Nakano, H. Miki, S. Nakanishi, H. Iba, T. Uchiyama, T. Watanabe, Y. Orikasa, K. Amezawa, Y. Uchimoto, *J. Mater. Chem. A*, 2021, **9**, 406–412.

[3] M. D. Reichert, M. A. White, M. J. Thompson, G. J. Miller, and J. Vela, *Inorg. Chem.* 2015, **54**, 6356–6362.

[4] H. J. Song, H. J. Shin, Y. Chung, J. C. Lee, M. K. Lee, *J. Appl. Phys.* 2005, **97**, 113711-7.

[5] L. Kjellsson, V. Ekholm, M. Agåker, C. Såthe, A. Pietzsch, H. O. Karlsson, N. Jaouen, A. Nicolaou, M. Guarise, C. Hague, J. Lüning, S. G. Chiuzbăian, and J.-E. Rubensson, *Phys. Rev. A*, 2021, **103**, 022812-7.

STUDY OF SOFT X-RAY EMISSION ANGULAR ANISOTROPY OF GAS PHASE

Naoya Kurahashi[1], Jun Miyawaki[2], Kosuke Yamazoe[3], Hisao Kiuchi[1], Wenxiong Zhang[1], Ugalino Ralph[1] and Yoshihisa Harada[1]

[1]*Synchrotron Radiation Laboratory, The Institute for Solid State Physics, The University of Tokyo*

[2] *National Institutes for Quantum Science and Technology*

[3]*Japan Synchrotron Radiation Research Institute*

Soft X-ray emission spectroscopy is a powerful technique to observe the electronic state of occupied orbitals, which emits excess energy as light when valence electrons relaxation to inner-holes generated by the excitation light of soft X-rays. The measurement under ambient pressure and measurement of wet samples are possible using the X-ray transmission window. In contrast, photoelectron spectroscopy is another method for directly observing occupied electron orbitals, and it is possible that photoelectron spectroscopy and emission spectroscopy provide complementary information, as exemplified by the results of bulk water measurements. While soft X-ray emission spectroscopy can measure samples in a variety of environments, it tends to have a broad natural width of the spectrum, due to the short lifetime of inner-holes. Because of this, it may not be possible to completely separate the electron orbitals, and a method for assigning electron orbitals other than emission energies is required.

Since photoelectron spectroscopy for atoms and molecular has long been used to study photo-excitation dynamics, there has been a need for a method to understand the electronic excitation states. To solve this problem, a photoelectron velocity mapping method[1] has been developed that enables simultaneous observation of the kinetic energy and emission angle of photoelectrons. In the process of photoelectron emission, the orbital angular momentum of electrons changes by ±1 according to the law of conservation of angular momentum. For example, electrons from the *s*-orbital are emitted in the form of *p*-orbitals, while those in the *p*-orbital are emitted as a superposition of *s*- and *d*-orbitals. As a result, by measuring the kinetic energy and emission angle distributions of photoelectrons, information on the energy levels and angular momenta of the original orbitals can be obtained, which enables precise assignment of electron orbitals.

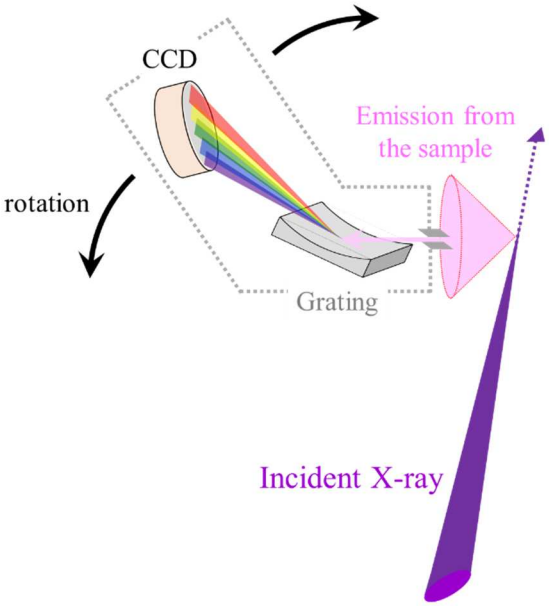

Fig. 1 Schematic of soft X-ray emission angular anisotropy measurement. The incident light and emission points were fixed and the spectrometer was rotated in the horizontal plane.

We have planned a soft X-ray emission angular anisotropy observation experiment on a gas-phase sample, because we thought that the electron orbital information could be obtained from the soft X-ray emission angular distribution in the same way as the photoelectron emission angular distribution has information on the orbital angular momentum (Fig. 1). By using a gas-phase sample, the angular emission anisotropy is considered to depend only on the angle between the molecular axis and the electric field plane of light (polarization) and the symmetry between the core-excited intermediate and final states of the molecule, making it easy to compare with theoretical calculations. In angle-resolved spectroscopy, it is necessary to consider the

lifetime of the intermediate state because the angle information is lost due to molecular rotation. However, in soft X-ray emission spectroscopy, the lifetime of the intermediate state is very short (few femto-seconds), and the positional relationship between the molecule and the light is considered to be conserved. Due to the trade-off between energy resolution and detection efficiency in emission spectroscopy, and the low efficiency of X-ray fluorescence for light elements, soft X-ray emission spectroscopy for gaseous samples has been considered difficult. To solve this problem, we have developed a high-density gaseous sample introduction method. This method enables us to introduce a high-density gas-phase sample into a very small area while maintaining a high vacuum in the measurement chamber.

Using the newly developed sample introduction method, we performed soft X-ray emission angle anisotropy observation of oxygen gas and succeeded in the first soft X-ray emission angle anisotropy measurement of gaseous molecules. The pressure in the vacuum chamber remained at around 10^{-4} Pa even though 100 kPa oxygen gas was introduced, and no influence on the light source or other devices was observed.

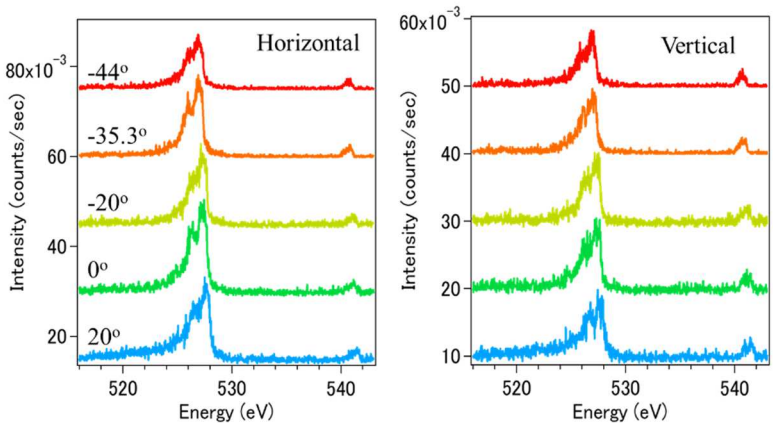

Fig. 2 Soft X-ray emission angle anisotropy measurements of oxygen excited at 541.3eV. The angle in the figure indicates the angle between the electric field plane of the excitation light and the monochromator.

The soft X-ray emission angular anisotropy at excitation energy of 530.8 eV, which is the π* excitation ($^3\Sigma_g^- \rightarrow {}^3\Pi_u$) was re-measured. In the case of horizontal polarization, the anisotropy parameters were -0.62±0.04 for $^3\Sigma_{g^-}$ emission and +0.23±0.15 for $^3\Pi_g$ emission. These values were close to the respective anisotropy parameters of -0.57 and +0.36 obtained from geometric calculations. From this result, it is concluded that the emission process of $^3\Pi_u$ excitation in oxygen gas is a dipole transition, which occurs sufficiently faster than the molecular rotation. Since the lifetime of $^3\Pi_u$ is expected to be highly dependent on the excitation energy, we would like to challenge the excitation energy dependence of $^3\Pi_u$ angular anisotropy in the next beam time. On the other hand, no clear angular anisotropy was observed at 541.3 eV (Fig. 2), which is the Rydberg excitation, and it is possible that the molecular rotation cancels out the angular anisotropy because the excited state lifetime tends to be long due to the hydrogen atom-like electron configuration in the Rydberg excitation. However, no clear conclusion has been reached on the emission lifetime in this region due to a lack of examples of studies, so we would like to compare our results with theoretical calculations.

No angular anisotropy was observed in any of the peaks when the polarization was set to vertical. This indicates that the measurement system maintains cylindrical symmetry in longitudinal polarization. This means that the sample emission occurred at the center of rotation of the spectrometer and that the gas-phase sample measurement setup was successful.

With this study, we have successfully performed windowless experiments of soft X-ray emission spectroscopy of oxygen gas and measured the angular anisotropy of the soft X-ray emission. In the future, we would like to try soft X-ray emission angle anisotropy experiments of vaporized water, which is important for comparison with bulk water.

REFERENCES

[1] T. Suzuki, *Annu. Rev. Phys. Chem.*, 57, 555 (2006).
[2] J.-E. Rubensson *et al.*, *J. Electron Spectros. Relat. Phenomena*, 185, 294 (2012).

ELECTRONIC STATE ANALYSIS OF EARTH-ABUNDANT FE–AL–SI THERMOELECTRIC (FAST) MATERIALS USING SCANNING PHOTOELECTRON MICROSCOPY (II)

Yoshiki TAKAGIWA[1], Shunsuke TSUDA[1], Naoka NAGAMURA[1,2,3], Asako YOSHINARI[1,3], Shingo TAKEZAWA[1,3], Kenta OISHI[1,2,3], Kentaro FUKU[4], Wenxiong ZHANG[5]

[1]*National Institute for Materials Science (NIMS), Tsukuba, Ibaraki, Japan.*
[2]*PRESTO, Japan Science and Technology Agency, Honcho, Saitama, Japan.*
[3]*Tokyo University of Science, Katsushika, Tokyo, Japan*
[4]*Tohoku University, Sendai, Miyagi, Japan*
[5]*The University of Tokyo, Kashiwa, Chiba, Japan*

One of the unsolved global-scale issues is developing technology that effectively uses energy represented by unused waste heat. It is known that exhaust heat below 200°C occupies ~70% of the total. From this perspective, thermoelectric materials that can directly convert heat to electrical energy can be considered clean energy materials. Unfortunately, except for space and remote areas, our society has not yet implemented power generation using thermoelectric materials.

To develop environmentally friendly thermoelectric materials that are non-toxic and low-cost with sufficient power output to drive sensor devices, in particular, at a low-temperature region below 400 K, we developed FAST materials (**Fe**-**Al**-**Si** **T**hermoelectric Materials) composed of τ_1-$Fe_3Al_2Si_3$ phase forms a narrow bandgap of ~0.2 eV near the Fermi level [1]. We demonstrated that the Al/Si ratio fine-tuning could control its conduction type and enhance the power factor without chemical substitutions [2]. Relatively large power factors were obtained for p- and n-type thermoelectric materials below 400 K, which possessed high oxidation resistance and excellent mechanical properties [3]. Recently, we improved the power factor at mid-temperatures using machine-learning-assisted synthesis and evaluation by tuning the compositions [4,5]. Furthermore, we succeeded in the bonding technology to build a small-sized and highly integrated thermoelectric power generation module: the operation of temperature/humidity sensors and wireless transmission was performed [6] (Fig. 1). To better understand the intrinsic thermoelectric characteristics of FAST materials, the electronic structure, including the magnitude of the bandgap and formation of impurity states, needs to be experimentally investigated.

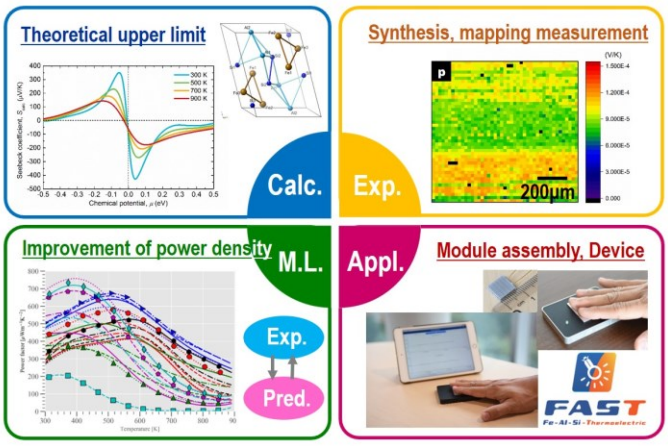

Fig. 1 Materials development, modularization technology, and power generation demonstration tests using experiment, mapping measurement, computational science, and machine learning.

In this work, we investigated the electronic structures of polycrystalline p- and n-type FAST materials by photoemission spectroscopy to obtain deeper insight into controlling the p-n characteristics to enhance the thermoelectric properties of FAST materials [7]. The core-level spectra of the p- and n-FAST materials for Al 2p, Al 2s, Si 2p, and Fe 3p are shown in Fig. 2, respectively. The solid curves are the raw spectra. For clarity, the spectra of the p-FAST material were by 0.15 eV toward the higher binding-energy side.

The photoemission spectra of the valence bands of the p- and n-FAST materials are shown in Fig. 3. Considering the photoemission cross section, these spectra strongly reflect Fe 3d orbitals. The dashed blue curve in Fig. 3 corresponds to the spectrum of the p-FAST material shifted by 0.15 eV toward higher binding energy. From Fig. 3, the energy positions of the highest intensities are almost the same. This indicates a rigid band shift owing to carrier doping by changing the Al/Si ratio.

We found that the photoemission spectra of the p- and n-FAST materials were consistent with the covalent bonding nature and semiconducting behavior. Because the core-level shifts were independent of the elements and orbitals, the observed chemical-potential change should be the dominant factor of the core-level shift of ~0.15 eV, close to the band gap of ~0.18 eV obtained from transport measurements.

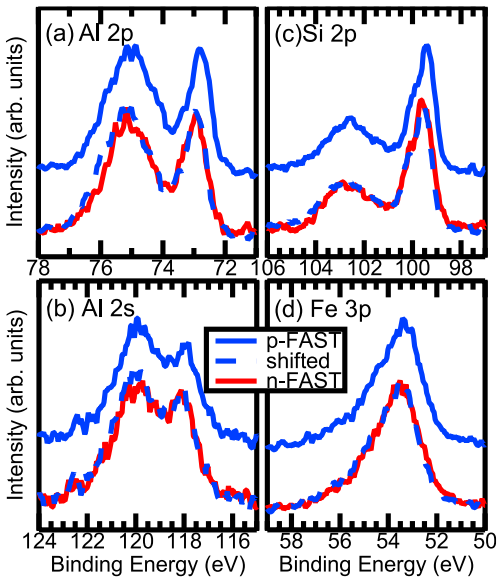

Fig. 2 Photoemission spectra of the (a) Al 2p, (b) Al 2s, (c) Si 2p, and (d) Fe 3p core levels. The blue (red) curves are the spectra of p-FAST (n-FAST) material. The solid curves are the raw spectra, and the dashed curves are the spectra shifted by 0.15 eV toward higher binding energy.

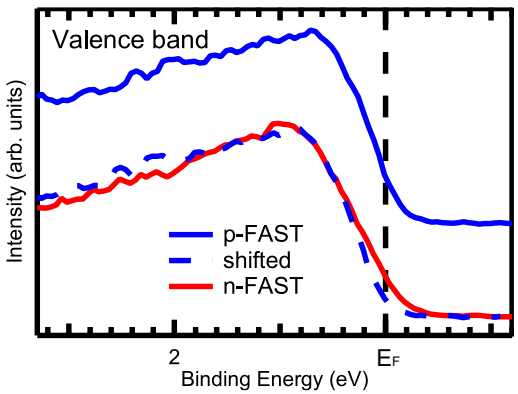

Fig. 3 Valence-band spectra of the p- and n-FAST materials. The blue and red solid curves are the spectra of the p- and n-FAST materials. The dashed blue curve is the spectrum of the p-FAST material shifted by 0.15 eV toward higher binding energy.

REFERENCES

[1] Y. Takagiwa, Y. Isoda, M. Goto, and Y. Shinohara, J. Therm. Anal. Calorim. **131**, 281 (2018).

[2] Y. Takagiwa, Y. Isoda, M. Goto, and Y. Shinohara, J. Phys. Chem. Solids **118**, 95 (2018).

[3] Y. Takagiwa and Y. Shinohara, Scripta Mater. **172**, 98 (2019).

[4] Z. Hou, Y. Takagiwa, Y. Shinohara, Y. Xu, and K. Tsuda, ACS Appl. Mater. Interfaces **11**, 11545 (2019).

[5] Y. Takagiwa, Z. Hou, K. Tsuda, T. Ikeda, and H. Kojima, ACS Appl. Mater. Interfaces **13**, 53346 (2021).

[6] Y. Takagiwa, T. Ikeda, and H. Kojima, ACS Appl. Mater. Interfaces **12**, 48804 (2020).

[7] S. Tsuda, A. Yoshinari, S. Takezawa, K. Ohishi, N. Nagamura, W. Zhang, Y. Iwasaki, and Y. Takagiwa, Mater. Res. Express **10**, 055506 (2023).

ANALYSIS OF ELECTRONIC CONFIGURATION FOR A WATER MOLECULE ENCAPSULATED INSIDE A FULLERENE

Yoshifumi Hashikawa,[1] Hisao Kiuchi,[2] Yoshihisa Harada[2]
[1]*Institute for Chemical Research, Kyoto University*
[2]*Synchrotron Radiation Laboratory, The Institute for Solid State Physics, The University of Tokyo*

Introduction. Water clusters found in hydrophobic subnanospaces such as graphitic interlayers and cavity of carbon nanotubes have been revealed to exhibit distinct properties essentially different from those in a bulk environment. For such water, the induction/expression of their functions and properties is heavily dependent on their physical and electronic structures offered by intermolecular hydrogen-bondings whilst authentic physical nature of water, i.e., a single water molecule without any hydrogen-bonding, has still remained unrevealed. To tackle this issue, in 2011, we have synthesized $H_2O@C_{60}$ where a single water molecule was isolated within a fullerene C_{60} cavity.[1] The X-ray absorption spectroscopy (XAS) and X-ray emission spectroscopy (XES) at O K-edge are powerful approaches to clarify the nature of water. In addition, resonant inelastic X-ray scattering (RIXS) measurement by an emission spectrometer with a high energy resolution could provide a potential energy surface of the molecule of target, thus revealing an effect of the environment surrounding the water molecule. Hence, these measurements are expected to be a crucial clue to probe the interaction between the water molecule and the carbon wall. Herein, we report our preliminary results on the physical nature of a single water molecule inside C_{60}.

Experimental methods. First, a powdery sample of $H_2O@C_{60}$ was moulded in a shape of a φ7 pellet by applying a hydraulic press. The measurements of O K-edge XAS, XES, and RIXS were performed at room temperature (SPring-8 BL07LSU). The XAS spectra were taken with a partial fluorescence yield mode using SDD (silicon drift detector). The XES and RIXS spectra were recorded with scanning the pellet sample for reducing a local sample damage by the irradiation with a small beam spot size of 7 μm × 50 μm.

Results and discussion. Figure 1 shows O 1*s* XAS and XES spectra of $H_2O@C_{60}$ as well as those for water reported previously.[2] In the XAS spectra, the energy shifts of molecular orbitals were observed with vanishing a Rydberg band (Figure 1b). This likely arises from a hybridization of widely distributed molecular orbitals of H_2O with those of C_{60}. Upon seeing the XES spectra, the emission band corresponding to a transition from

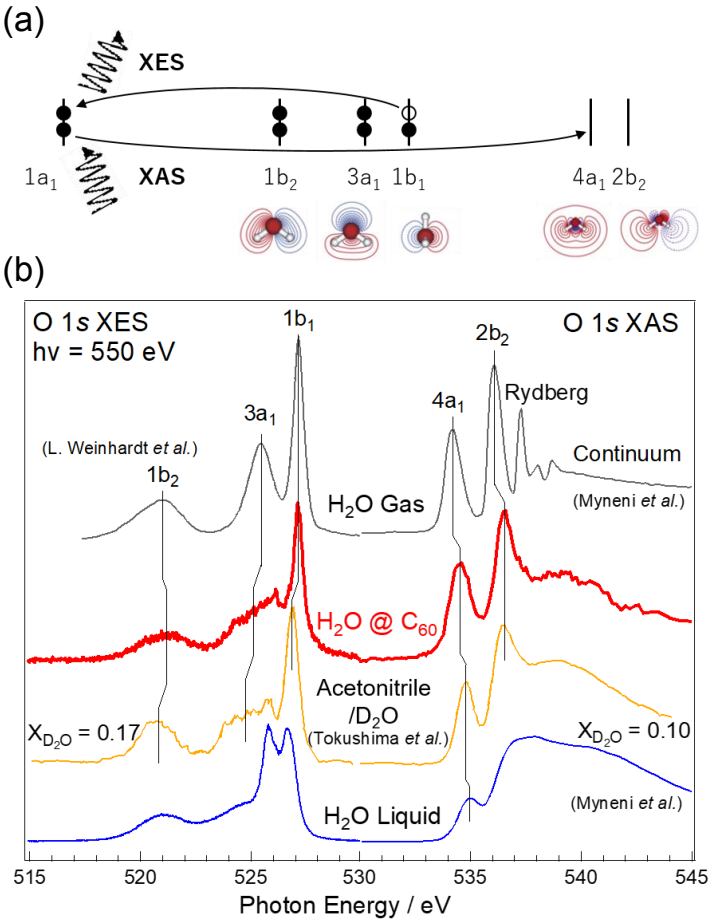

Figure 1. (a) Molecular orbital diagram of water and (b) XAS and XES spectra of $H_2O@C_{60}$ and previous reports.

$3a_1$ where the electron cloud is aligned in an axis of an electric dipole moment was found to be significantly broadened (Figure 1b). This is suggestive of the polarization shielded by the C_{60} cage. To get further insights into this phenomena, the theoretical calculations are currently ongoing.

Figure 2 illustrates RIXS spectra at the $4a_1$ and $2b_2$ resonances of $H_2O@C_{60}$ as well as gaseous water[3] reported previously, both of which showed multiple modes of vibration. Compared with gaseous water, the larger deviation of the peaks were confirmed for $H_2O@C_{60}$ at higher energy loss area. This is demonstrative of the flattening of a potential energy surface at higher energy levels. This is considered to be caused by the attractive interaction present between the single molecule of H_2O with the C_{60} wall, which might promote a water dissociation within the C_{60} cavity.

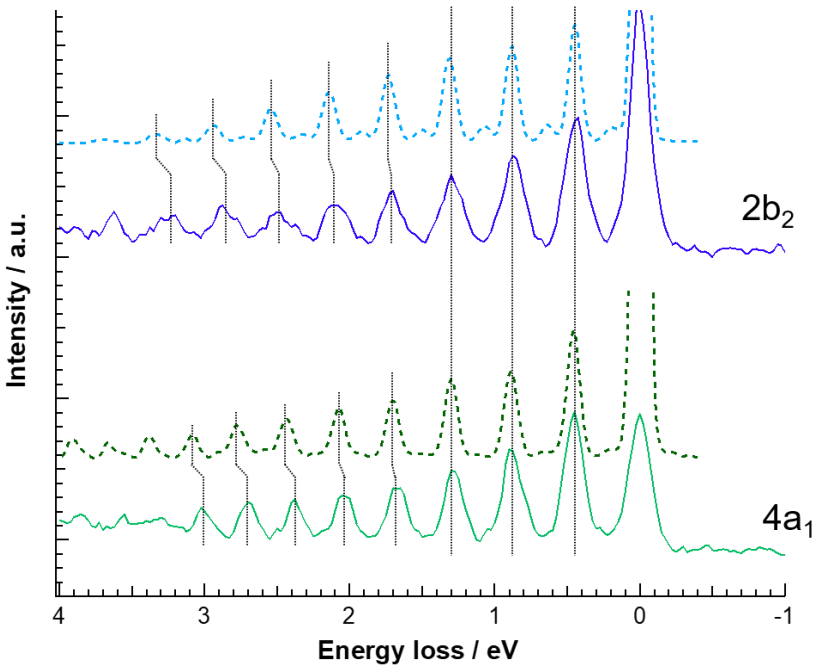

Figure 2. RIXS spectra of $H_2O@C_{60}$ (solid curve) and gaseous H_2O[3] (dashed curve).

Conclusion. We examined the electronic properties of $H_2O@C_{60}$ by XAS, XES, and RIXS measurements at SPring-8 BL07LSU. The XAS spectra showed a band shifts as well as a vanished Rydberg band, implying the presence of an orbital–orbital interaction between H_2O and C_{60}. This interaction was revealed to be attractive by RIXS measurements suggesting the flattening of a potential energy surface at higher energy levels. The additional measurements and theoretical studies are in progress for further understanding the nature of a single molecule of H_2O.

REFERENCES

[1] (a) Kurotobi, K.; Murata, Y. *Science* **2011**, *333*,613–616. (b) Hashikawa, Y.; Kizaki, K. Hirose, T.; Murata, Y. *RSC Adv*. **2020**, *10*, 40406–40410.

[2] (a) Weinhardt, L.; Benkert, A.; Meyer, F.; Blum, M.; Wilks, R. G.; Yang, W.; Bär, M.; Reinert, F.; Heske, C. *J. Chem. Phys*. **2012**, *136*, 144311. (b) Tokushima, T.; Harada, Y.; Takahashi, O.; Senba, Y.; Ohashi, H.; Pettersson, L. G. M.; Nilsson, A.; Shin, S. *Chem. Phys. Lett*. **2008**, *460*, 387–400. (c) Myneni, S.; Luo, Y.; Näslund, L. Å.; Cavalleri, M.; Ojamäe, L.; Ogasawara, H.; Pelmenschikov, A.; Wernet, P.; Väterlein, P.; Heske, C.; Hussain, Z.; Pettersson, L. G. M.; Nilsson, A. *J. Phys. Condens. Matter* **2002**, *14*, L213–L219.

[3] Cruz, V. V. d.; Ertan, E.; Couto, R. C.; Eckert, S.; Fondell, M.; Dantz, M.; Kennedy, B.; Schmitt, T.; Pietzsch, A.; Guimarães, F. F.; Ågren, H.; Gel'mukhanov, F.; Odelius, M.; Föhlisch, A.; Kimberg, V. *Phys. Chem. Chem. Phys*. **2017**, *19*, 19573–19589.

Electrolyte Dependence of the Mn 3*d* Electronic Structure of $LiMn_2O_4$ Cathode Studied by Soft X-ray Emission Spectroscopy

Daisuke Asakura[1,2], Yusuke Nanba[1], Eiji Hosono[2,3], Hideharu Niwa[4], Hisao Kiuchi[4], Jun Miyawaki[4], and Yoshihisa Harada[2,4]

[1]*Research Institute for Energy Conservation, National Institute of Advanced Industrial Science and Technology (AIST)*

[2]*AIST-UTokyo Advanced Operando-Measurement Technology Open Innovation Laboratory, AIST*

[3]*Global Zero Emission Research Center, AIST*

[4]*Synchrotron Radiation Laboratory, The Institute for Solid State Physics, The University of Tokyo*

Li-ion battery (LIB) is one of the key energy-storage devices for CO_2 reduction and realization of sustainable society. To further enhance the performances of LIBs for applications to electric vehicles and large-scale stationary energy storage systems, increasing the charge-discharge capacity of the cathode is highly desired. Electronic-structure analysis using X-ray spectroscopy has been playing an important role on the clarification of the redox mechanism of cathode materials for LIBs, which will lead to increase of the charge-discharge capacity. By clarifying the redox mechanism of typical cathode materials, it is expected to obtain strategies to design novel cathode materials.

We have been studying the electronic structure of several cathode materials using soft X-ray absorption (XAS) and emission spectroscopy (XES). For example, the Mn *L*-edge XAS and XES studies for $LiMn_2O_4$, which is a prototypical cathode material, revealed the redox reaction of $Mn^{3+} \Leftrightarrow Mn^{4+}$ at the Mn^{3+} site in the initial state. The Mn^{4+} state has very strong charge-transfer (CT) effect between the O 2*p* and Mn 3*d* orbitals, resulting in the important role of O 2*p* orbital on the redox reaction.[1,2] These studies have been investigated for the charge-discharge reaction with a conventional organic electrolyte solution, 1-mol$\cdot$ dm^{-3} $LiClO_4$/ethylene carbonate (EC)-diethyl carbonate (DEC).

On the other hand, it is well known that $LiMn_2O_4$ could exhibit charge-discharge reaction with aqueous electrolyte solutions.[3] The usage of aqueous electrolyte solutions is advantageous in terms of safety (non-flammable) and manufacturing cost, while the working voltage is reduced to around 1.0 V (in contrast to ~4.0 V for organic electrolyte solutions) because of the narrow voltage window of H_2O. To investigate the redox reaction of $Mn^{3+} \Leftrightarrow Mn^{4+}$ in the case of aqueous electrolyte solution, we performed Mn *L*-edge XES studies for $LiMn_2O_4$ with 1-mol$\cdot$ dm^{-3} $LiNO_3/H_2O$.[4]

Powdered $LiMn_2O_4$ sample was fabricated by a sol-gel method.[2,4] The *operando* XES measurements with the aqueous electrolyte solution were carried out by HORNET spectrometer at BL07LSU, SPring-8. The setup of *operando* cell and details of the electrochemical measurements for *operando* XES are described in Ref. 4. To analyze the XES spectra, we conducted configuration-interaction full-multiplet (CTM) calculations.[2,4]

Figure 1 shows a comparison of the Mn L_3-edge XES spectra between the cases of the aqueous and organic electrolyte solutions. The line shape for the initial state is identical because the powder samples were fabricated with the same method. As described in Ref. 2, the initial state has been attributed to a mixed state of Mn^{3+} and Mn^{4+}. In contrast, the line shape after the first charge-discharge cycle is considerably different between the cases of aqueous (spectrum A) and organic (spectrum B) electrolyte solutions, indicating that the redox reaction is dependent on electrolyte. For the organic electrolyte solution, spectrum B is similar to the spectrum of the initial state, while the sample after the charge-discharge has

been measured under an *ex situ* condition.[2] This result indicates that the redox reaction with the organic electrolyte solution is relatively reversible for the first cycle. For the aqueous electrolyte solution, the redox reaction for the first cycle is irreversible. However, CTM calculations revealed that spectrum A also consist of Mn^{3+} and Mn^{4+}.[4] The difference from spectrum B is mainly originated from the charge-transfer energy Δ (from O 2*p* to Mn 3*d* orbitals) for each Mn^{3+} and Mn^{4+}.[4]

The *operando* XES results after the second cycle with the aqueous electrolyte solution (not shown here) were similar to those after the first cycle,[4] indicating that the second cycle is reversible. The change from the spectrum of the initial state to spectrum A suggests formation of surface-electrolyte interface (SEI) layer characteristic of the aqueous electrolyte solution, while SEI layer is also formed for the cases of organic electrolyte solutions. Thus, after that the SEI layer is once formed on the first cycle, the reversibility of the redox reaction with the aqueous electrolyte solution should be enhanced.

As above, difference of electrolytes causes different redox reaction. The SEI layer formed by the charge-discharge should strongly affect the electronic structure of cathode materials. We will try to the Mn *L*-edge *operando* XES of $LiMn_2O_4$ with solid-state electrolyte as all-solid-state battery.[5] The $LiMn_2O_4$/solid-state electrolyte interface is expected to be completely different from the $LiMn_2O_4$/liquid electrolyte interfaces. Thus, the redox reaction with solid-state electrolytes should be verified in the future.

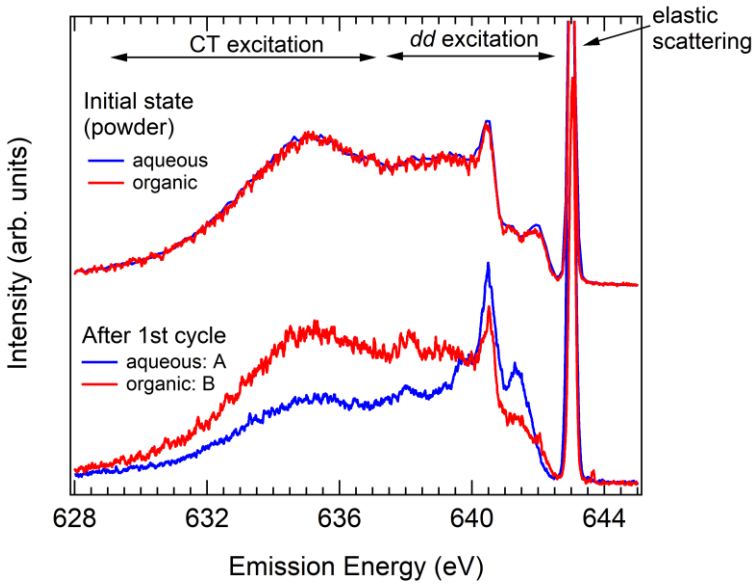

Fig. 1. Mn L_3-edge XES spectra for $LiMn_2O_4$ with the cases of aqueous and organic electrolyte solutions. The initial state corresponds to the powder sample before charge-discharge for both electrolytes. Spectra A and B after the first cycle were measured under *operando* and *ex situ* conditions, respectively.[2,4] The excitation energy was 643.0 eV.

REFERENCES

[1] D. Asakura *et al*., Electrochem. Commun. **50**, 93 (2015).
[2] D. Asakura *et al*., Phys. Chem. Chem. Phys. **21**, 18363 (2019).
[3] For example, W. Pei *et al*., J. Power Sources **63**, 275 (1996) and V. A. Nikitina *et al*., Langmuir **33**, 9378 (2017).
[4] D. Asakura *et al*., Phys. Chem. Chem. Phys. **24**, 19177 (2022).
[5] For example, H. Kitaura *et al*., J. Electrochem. Soc. **157**, A407 (2010).

SOFT X-RAY STRUCTURAL ANALYSIS OF CONSTRAINED WATER MOLECULES ON NICKEL-COMPLEX ANION SALT AGGREGATES

Tomoko Fujino
The Institute for Solid State Physics, The University of Tokyo

Introduction

Open-shell π/d-conjugated complexes have electron-rich structures and diverse electronic functionalities, including optical and magnetic properties. By combining the central metal and ligand, the electronic structure of these complexes can be precisely adjusted. When these complexes are assembled with effective intermolecular interactions such as π–π interactions, they form band structures that exhibit different electronic functionalities from those in the isolated form, including electrical and magnetic conductivities. We focused on assembling electronically charged open-shell complexes, which offer benefits such as hydrophilicity that enhance their fabrication applicability in environmentally friendly electronic devices. These charged complexes also provide structural diversification in assembled structures and functions depending on the variations of counter ions. However, these complexes are still rare even despite several decades of research because electrostatic repulsion between charged molecules severely hampers their assembly, except for charge-transfer complexes in segregated stacks between donors and acceptors. Only a few examples, such as $[M(dmit)_2]^{2-}$ (dmit = 2-thioxo-1,3-dithiol-4,5-dithiolate, M = Ni, Pd, Pt, etc) anion salts, have succeeded in exhibiting a tightly π-stacked form, resulting in properties such as unique magnetic characteristics, near-IR absorption, and superconductivity under high pressures.

We previously developed neutral metal dithiolene complexes with electron-donating substituents on their side chains [1,2]. These complexes displayed conductive properties when assembled in single crystals [1] or thin films [2] demonstrating the unique conductive properties, but not in isolated salt forms. We hypothesized that combining the hydrophilic precursors of the neutral complexes with hydrophobic counter cations that possess long-chain alkyl chains could form amphiphilic open-shell d/π conjugated complex anion salts. Such an amphiphilic structure may form macroscopic assemblies in aqua, exhibiting strong π–π interactions between complex anions. This mobile soft aggregate could demonstrate dynamic macro-sized structural changes responsive to the external environment. Therefore, we synthesized an amphiphilic salt of the d/π-conjugated complex anion with a hydrophobic counter cation possessing double dodecyl chains, which formed a macro-sized assembly where the complex anions showed considerable π–π stackings at room temperature, demonstrating rich conductive properties. The macrostructures exhibited temperature-dependent dynamical structural changes at approximately 65 °C, but the detailed mechanism in the properties remains unclear due to the lack of atomic-level structural information.

In this study, we investigated the origin of these unique electronic functionalities by Ni XAS at BL07LSU, which was developed by Prof. Harada's group. By using Ni XAS, we analyzed the electronic characteristics and temperature dependency of an aqueous solution of the complex anion salts flowing in the system. Our analysis showed that at lower temperatures than the transition temperature, the suspended solution displayed a spectrum with two peaks at the Ni L3 absorption edge, unlike the isolated forms of complex anions, where only a higher-energy peak was observed. We suspect the lower-energy peak may be a result of possible intermolecular Ni–Ni interactions. When the temperature was raised above

the transition temperature of the dynamical change, the lower-energy peak disappeared, but it reappeared when the solution was cooled again. It appears that the interactions between Ni elements disappeared when the assembled form was released. This is likely consistent with the observation of high-temperature small- and wide-angle X-ray scattering that showed macro-sized assembly was released, resulting in the loss of the formed band structures based on the intermolecular π–π stacking. The intramolecular structural details were further addressed with the wide-ranged XAS measurements covering the energy ranges for Ni L3 and L2 absorption edges. At 80 °C, charge-transfer satellite peaks appeared on L3 and L2 absorption edges, but not at low temperatures. This indicates that intramolecular charge transfer occurred from the ligand to the central metal when the assembly was released into the isolated form at high temperatures. These findings confirmed that the release of the macro-sized assembly caused changes in the loss of intermolecular Ni–Ni interactions, altering the intramolecular electronic structure.

This work was supported by Prof. Yoshihisa Harada, Dr. Hisao Kiuchi, and Dr. Naoya Kurahashi (ISSP, The Univ. of Tokyo) for their support on XAS measurements and fruitful discussions. We appreciate their kind and professional suggestions. We also thank Assoc. Prof. Mafumi Hishida (ISSP, The Univ. of Tokyo) for small- and wide-angle X-ray scattering measurements. We appreciate Prof. Hatsumi Mori and Mr. Masatoshi Ito (ISSP, The Univ. of Tokyo) for the synthesis support and considerable discussions. This work was partially supported by JSPS Grants-in-Aid for Scientific Research (JP20H05206, JP21K05018, JP22H04523), JST PRESTO (JPMJPR22Q8), a research grant from Naito Foundation, the Kao Foundation for Arts and Science.

REFERENCES

[1] Yokomori, S.; Dekura, S.*; Fujino, T.; Kawamura, M.; Ozaki, T.; Mori, H.* *J. Mater. Chem. C* **2020**, *8* (42), 14939-14947.

[2] Ito, M.; Fujino, T.*; Zhang, L.; Yokomori, S.; Higashino, T.; Makiura, R.; Takeno, K. J. Ozaki, T.; Mori, H.* *J. Am. Chem. Soc*., **2023**, *145* (4), 2127–2134.

AMBIENT PRESSURE X-RAY PHOTOELECTRON SPECTROSCOPY STUDY OF THE ELECTRONIC STATES OF THE MoS_2 BASAL PLANE DURING ANNEALING IN HYDROGEN

Fumihiko Ozaki, YoungHyun Choi, Wataru Osada, Yoshiko Sakaguchi, Shunsuke Tanaka, Kozo Mukai, Masafumi Horio, Iwao Matsuda and Jun Yoshinobu
The Institute for Solid State Physics, The University of Tokyo

Introduction

Molybdenum disulfide (MoS_2) has attracted attention in various applications such as gas sensors, field-effect transistors, and optoelectronic devices due to its unique optical properties and high carrier mobility. A formation of sulfur vacancies on the MoS_2 surface plays an important role in device performance because the electronic state is affected by sulfur vacancies [1]. In addition to these applications, MoS_2 has also been used as a catalyst for a variety of other applications, including hydrogenated desulfurization (HDS) catalysts. The sulfur vacancies serve as adsorption sites for molecules such as organosulfur compounds [2].

Many studies have been conducted to characterize the properties of sulfur vacancies. In particular, the electronic properties of MoS_2 surfaces with sulfur vacancies have been investigated by X-ray photoelectron spectroscopy (XPS) [3]. The XPS spectra of the core-levels show the chemical components associated with the sulfur vacancies. Quantitative explanations for this chemical shift are lacking, and the electronic state of sulfur vacancies is not fully understood yet.

Annealing in hydrogen is one of the methods of sulfur vacancy formation; adsorbed hydrogen atoms are reacted with and sulfur and desorbed as H_2S above 600 K, leading to the formation of sulfur vacancies [4]. In this study, ambient pressure (AP-) XPS measurements of the MoS_2 basal plane were performed to clarify the electronic state during annealing in hydrogen, and it is found that at the HDS reaction temperature of 600 K, a low-binding energy component appears in both the Mo 3d and S 2p spectra. Furthermore, the intensity ratio of the Mo 3d and S 2p spectra (S 2p/Mo 3d) decreases dramatically at 600K. This indicates the formation of sulfur vacancies on the MoS_2 basal plane.

Experimental

A natural MoS_2 single crystal was used as a sample (ALLIANCE Biosystems; about 50 mm^2, 0.5 mm thick). After mounting the sample on a metal plate, surface layers were peeled off in air using Scotch tape. Within 10 minutes after peeling, the sample was transferred to a load lock chamber and annealed in an ultra-high vacuum chamber at about 550 K for 30 minutes. AP-XPS measurements were performed in a chamber equipped with a hemispherical electron energy analyzer at SPring-8 BL07LSU. High-purity H_2 gas was introduced into the gas cell and the sample was slowly heated in H_2 from 302 K to 750 K for a total of 2.5 hours. All XPS spectra were obtained using a photon energy of 680 eV. The binding energies of the measured XPS spectra were calibrated using the Fermi level of a gold foil attached to the sample holder.

Results and discussion

Initially, 1.5 mbar of hydrogen gas was introduced into the gas cell, and then a sample temperature was increased from 302 K to 750 K. Figure 1 show the AP-XPS spectra of Mo 3d, S 2p, and valence band as a function of sample temperature, respectively. The intensity ratio of the S 2p core level to the Mo 3d core level is also shown in Figure 2. The peak energies of the Mo 3d core-level, the S 2p core-level, and the valence band uniformly shift to a lower binding energy of about 0.2 eV up to 600 K. Judging from this uniform energy shift, it can be

attributed to band bending in the MoS_2 crystal [5]. Furthermore, the S 2p/Mo 3d intensity ratio is almost constant up to 600 K, indicating that the HDS reaction does not occur.

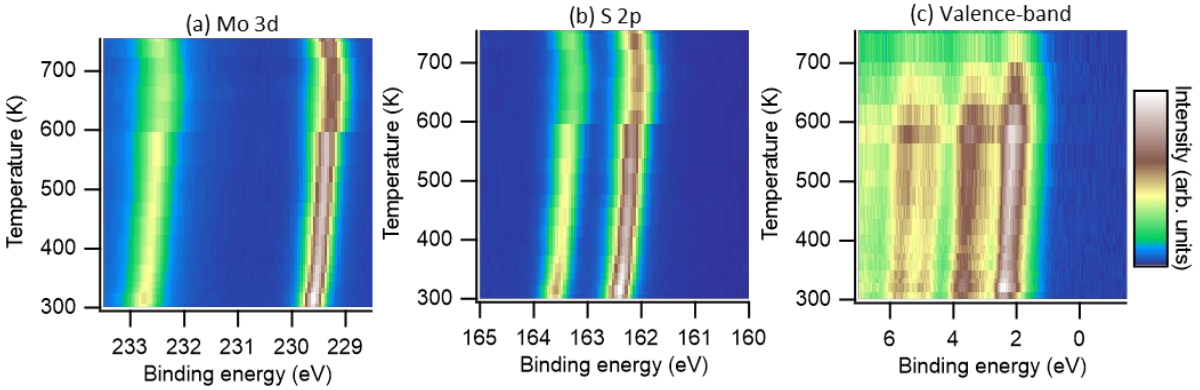

Figure 1. (a) Mo 3d, (b) S 2p, (c) Valence-band AP-XPS spectra of the MoS_2 basal plane as a function of the sample temperature in H_2 gas of ~1.5 mbar. The sample temperature increased from 302 K up to 750 K.

After 600 K heating, the peaks shift to lower binding energy and their widths become significantly broadened. This indicates the appearance of a new component in the Mo 3d and S 2p spectra. Furthermore, the S 2p/Mo 3d intensity ratio decreases markedly above 600 K, indicating that the HDS reaction takes place as indicated by the previous studies [6]. Hence, the new component observed in the Mo 3d and S 2p spectra may be related to the formation of sulfur vacancies.

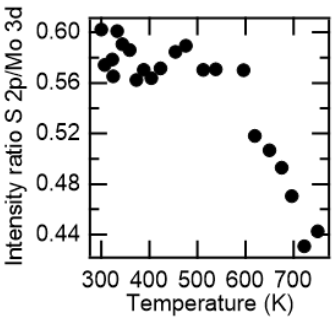

Figure 2. Plot of the S 2p/Mo 3d intensity ratio.

To clarify the spectral changes with new components, a comparison of the XPS spectra at 538 K and 619 K shows a decrease in intensity around 229.38 eV (162.21 eV) and an increase around 229.13 eV (161.88 eV) for Mo 3d (S 2p). Such a lower binding energy shift implies an increase in electron density at the Mo and S atoms. The electrons left on the MoS_2 surface by the desorption of sulfur as H_2S would be redistributed to the surrounding atoms. This interpretation has been supported by our recent first-principles calculations including the estimation of absolute binding energies based on the several defect models as well as AP-XPS data [7].

Acknowledgments

The AP-XPS measurements using synchrotron radiation were performed at SPring-8 BL07LSU as joint research between the Synchrotron Radiation Research Organization and The Institute for Solid State Physics, The University of Tokyo (Proposal No. 2022A7449, 2021B7432).

REFERENCES

[1] M. D. Siao *et al*., Nat. Commun. **9**, 1442 (2018).
[2] R. V. Mom *et al*., Nat. Commun. **10**, 2546 (2019).
[3] S. W. Han *et al*., Phys. Chem. Chem. Phys. **21**, 15302 (2019).
[4] X. S. Li *et al*., J. Catal. **137**, 385 (1992).
[5] F. Ozaki *et al*., Appl. Surf. Sci. **593**, 15 (2022).
[6] A. Bruix *et al*., ACS Nano **9**, 9322 (2015).
[7] F. Ozaki et al., submitted (2023).

BAND BENDING AT (001) AND (101) INTERFACES OF ANATASE PARTICLE REVEALED BY MICROSCOPIC X-RAY PHOTOELECTRON SPECTROSCOPY

Wenxiong Zhang[1], Mustafa Al Samarai[1], Hisao Kiuchi[1], Daobin Liu[1], Haochong Zhao[1], Fangyi Yao[2], Qi Feng[2], Yoshihisa Harada[1]

[1] *The Institute for Solid State Physics, The University of Tokyo*

[2] *Department of Advanced Materials Science, Kagawa University*

Titanium dioxide (TiO_2) has been used in many technological areas, including photocatalysis, solar cells, gas sensors, etc. Among different polymorphs (brookite, anatase, and rutile), anatase TiO_2 is considered a superior photocatalysis due to its higher electron mobility and longer carrier lifetime. It was reported that the (001) and (101) facets co-exposed anatase particles showed highly improved photocatalytic properties.[1] Theoretical calculation and experimental results on the (001) and (101) facets-exposed thin films have demonstrated that a surface heterojunction would be formed between two facets due to their difference in the Fermi levels.[2,3] As a result, photogenerated electrons and holes could accumulate on the interface of the (101) and (001) facets, therefore exhibiting different photocatalytic properties on these facets. For a deeper understanding of the charge separation mechanism of anatase TiO_2, a microscopic X-ray photoelectron spectroscopy (XPS) with spatial resolution better than 100 nm is employed to elucidate the facet-dependent electronic structure of micron-sized anatase TiO_2 particle.

Figure 1a shows the Ti 2*p* photoelectron intensity mapping image of the anatase TiO_2 particle. The particle exhibits a truncated octahedral bipyramid morphology, which is consisted of eight {101} facets on the sides and two {001} facets on the top and bottom. The geometrical relationships between the photoelectron analyzer and the incident beam spot on the sample caused the intensity difference in the mapping image.[4] Figures 1b and 1c show the pinpoint O 1*s* and Ti 2*p* XPS spectra shown in the enlarged area of the orange square (Fig. 1a) respectively. The consecutive 4 spots (~100 nm^2 each) cover the (101) and (001) facets of the anatase particle, as well as the interface between them. It is noted that the O 1*s* and Ti 2*p* XPS spectra of anatase TiO_2 continuously shift to the low binding energy from the (101) facet to the (001) facet. Figure 1d shows that the valence band maximum exhibits the same tendency as O 1*s* and Ti 2*p* XPS spectra, suggesting a smaller binding energy of the valence band maximum for the (001) facet. As a result, the interface areas for both (101) and (001) facets were calculated to be ~50 and ~80 nm respectively according to the dotted fitting spectra results (Fig. 1d). It can be concluded that a band bending (space charge layer of 130 nm) between (001) and (101) facets could be formed due to the difference of the valence band maximum between the (101) and (001) facets, hence, the photogenerated electrons and holes could accumulate on the interface, thereby exhibiting enhanced photocatalytic activities. For the strategy of morphology control to improve the photocatalysis performance of TiO_2, microspectroscopy using synchrotron soft X-ray is an important technique.

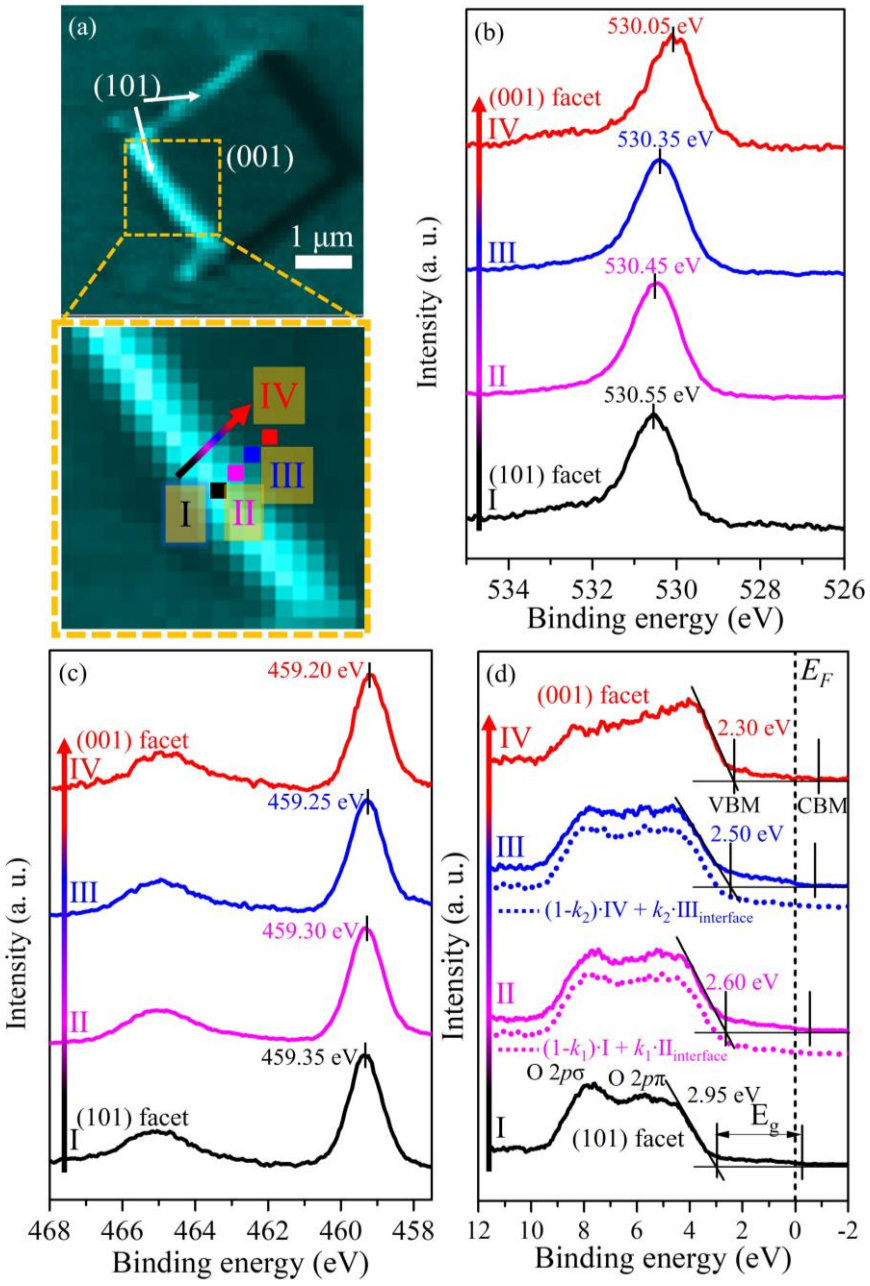

Figure 1. (a) Ti 2*p* photoelectron intensity mapping image of anatase TiO_2 particle and its enlarged area of the orange square. Pinpoint (b) O 1*s*, (c) Ti 2*p*, and (d) valence band XPS spectra of TiO_2 particle from consecutive 4 spots shown in Fig. 1a. CBM: conduction band minimum. VBM: valence band maximum. E_g: band gap energy. Norm.: normalization. *CBM is only speculation according to E_g = 3.2 eV. k_1 = 0.5 (0.5 x 100 nm = 50 nm, interface at area II). k_2 = 0.8 (0.8 x 100 nm = 80 nm, interface at area III).

REFERENCES

[1] H. G. Yang et al., *Nature*, 453 (2008) 638-642
[2] J. Yu et al., *J. Am. Chem. Soc.*, 136 (2014) 8839-8842
[3] S. Kashiwaya et al., *Adv. Energy Mater.*, 8 (2018) 1802195
[4] W. Zhang et al., *CrystEngComm.*, 25 (2023) 183-188

Influence of surface charge induced by ultrafine water on trans-epidermal water retention of stratum corneum lipids explored by O *K*-edge spectroscopy

Mustafa al Samarai[1], Wenxiong Zhang[1], Hisao Kiuchi[1], Shinsuke Inoue[2], Yuki Tabata[2], Hiroto Kato[2], and Yoshihisa Harada[1]

[1]*Synchrotron Radiation Laboratory, The Institute for Solid State Physics, The University of Tokyo*
[2]*Innovation center, Aisin Corporation.*

In recent years, nanosized water clusters called ultrafine water (UFW), which have several nanometers or less diameter, have attracted attention for their wide range of functions such as humidification, moisture retention, deodorization, air cleaning and sterilization, and static electricity removal. However, little is known about the mechanism of their functions. For example, in moisturizing, penetration into the subcutaneous tissue is considered because the UFW is smaller than the intercellular space on the skin surface. However, this alone cannot account for the long-lasting moisturizing effect [1]. Therefore, it is necessary to clarify the physicochemical properties of UFW to understand those macroscopic functions. In this study, a mixed-lipid bilayer model (artificial skin) of stratum corneum film (consisting of ceramide, cholesterol, and palmitic acid in a 1:1:1 molar ratio and approx.12.5 nm thick) was prepared on Au-coated 150 nm thick SiC membrane. We investigated the electronic structure of absorbed UFW vs. water by regular humidification at 60% relative humidity (RH) on the artificial skin using O *K*-edge XAS and XES to obtain detailed information on the hydrogen-bonded configuration of water on those surfaces, and to discuss the relationship between the chemical state and the function of UFW. XAS/XES will represent unoccupied/occupied valence electronic structures of water, which is quite sensitive to various hydrogen-bonded configurations in water [2].

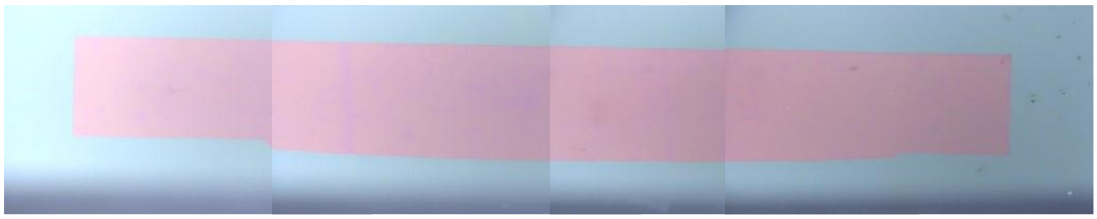

Figure 1: Photo image of the artificial skin prepared on a 150 nm thick SiC membrane (purple area); it was a key to make an uniform layer on the Au-coated membrane at 12.5 nm thickness where interference fringes were completely invisible.

The summary of the XAS/XES data for humidification by either UFW or 60%RH is shown in Fig. 2. Based on the combination of the obtained data, an obvious extraordinary increase of hydration in the artificial skin by flowing UFW was confirmed compared to regular

humidification at 60%RH. For both identical samples the O *K*-edge XAS and XES for the dry state were measured (black curves in Fig. 2) followed by the humification either by UFW vs. 60%RH. Finally, the samples were redried to investigate the nature of the trapped water within or on the artificial skin samples.

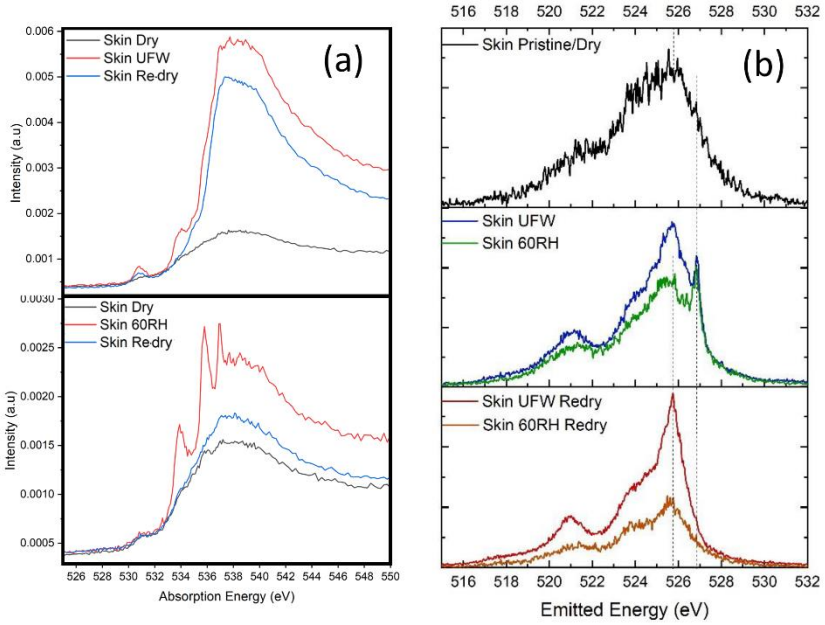

Figure 2. O K-edge (a) XAS and (b) XES for Dry artificial skin (black) under humidification by UFW vs regular humidification at 60%RH. Retention of hydration is reflected in the Redry data.

The surface to volume ratio in the smaller UFW water clusters (~ 1nm) is four orders of magnitude higher than the water mist (~ 10μm in diameter) found in the regular humidified gas flows. Therefore we expected different water absorption behavior and amount for the UFW humidification. For both the humidification pathways there are dominantly two water species, the gas phase water (at ~534 eV and ~526.9 eV in Figs. 2a and 2b) and trapped water (at ~538 eV and ~525.8 eV in Figs. 2a and 2b). Hereby, first the gas phase water is dominant especially in the 60%RH case, followed by the gradual isotropic equilibrium shift towards precipitation of additional water from the vapor to the already present water domains on the surface of artificial skin and trapped within the lipid bilayer. Interestingly we see a higher water /humidification absorption for the UFW-treated sample. Furthermore, following the redrying process a considerably higher amount of water was retained for the UFW treated sample relative to the regularly humidified (60%RH) sample.

This experimental evidence suggests that initial humidification with UFW produces water adsorption sites on the hydrophobic skin surface. In the future, by accumulating data under more specific conditions, we can identify the coordination of various water layers and the involved chemical bonds, which will help design the function of novel UFW.

REFERENCES

[1] N. Nishimura *et al*., Skin Res. Technol. **25**, 294 (2019).
[2] T. Tokushima *et al.*, Chem. Phys. Lett. **460**, 387 (2008).

2p3d Resonant Inelastic X-ray scattering Probing Ligand Field Perturbations in Fe-modified Co spinels

Minmin Chen,[1] Marcos Sepulcre,[1] Dimitrios Manganas,[2] Steven Angel,[3] Eko Budiyanto,[2] Derek Rice,[1] Harun Tüysüz,[2] Hartmut Wiggers,[3] Naoya Kurahashi,[4] Yoshihisa Harada,[4,5] Olaf Rüdiger,[1] Serena DeBeer[1]

[1] Max Planck Institute for Chemical Energy Conversion, 45470 Mülheim an der Ruhr, Germany

[2] Max-Planck-Institut für Kohlenforschung, 45470 Mülheim an der Ruhr, Germany

[3] University of Duisburg-Essen, 47057 Duisburg, Germany

[4] Institute for Solid State Physics, The University of Tokyo, Kashiwa, Chiba 277-8581, Japan

[5] Synchrotron Radiation Research Organization, The University of Tokyo, Sayo, Sayo-gun, Hyogo 679-5148, Japan

Spinels are an essential class of minerals which serve as fundamental structural models for advanced functional materials. Fe loading into spinels can significantly alter the physical-chemical properties of the parent spinel.[1] BET, XRD, APT, HRTEM, SAED, EELS, Raman spectroscopy and Mössbauer spectroscopy have been widely used to explore the role of Fe role in modulating morphology, crystal structure, oxidation state, and geometric structure. Recently, 2p3d RIXS has been used as a site-selective technique to probe the mixed-valence pure Co spinel.[2] Here we used 2p3d RIXS to directly probe the geometric and electronic environment surrounding a Co center in Fe-loaded Co-based spinels. $CoFe_2O_4$ (containing only $Co^{2+}(O_h)$), $CoAl_2O_4$ (containing only $Co^{2+}(T_d)$), and $ZnCo_2O_4$ (containing only $Co^{3+}(O_h)$) were chosen as references to study the spectral signatures of the different sites. Ligand-field multiplet calculations were used to reproduce the L-edge XAS and 2p3d RIXS of the references.[3] The calculated Tanabe-Sugano diagrams allow for the ligand field modulations of the low-lying excited states to be visualized. These electronic structure changes can then be correlated with the differences in Fe-induced electrocatalytic performance.

Figure 1 shows both L-edge XAS and 2p3d RIXS can distinguish Co^{2+} with different site symmetries (T_d vs. O_h), but 2p3d RIXS exhibits higher resolution and it is more sensitive to modulations in the ligand field splitting. Co^{2+} is excited primarily at lower incident energies (<780eV) than the Co^{3+} ions. Visually assigning characteristic inelastic features is a challenge. Herein, we utilize ligand-field-theory calculations within the ORCA code in order to reproduce experimental spectra of the references (Figure 2). In addition, the contributions from different multiplets can be deconvoluted based on the calculated spectra.

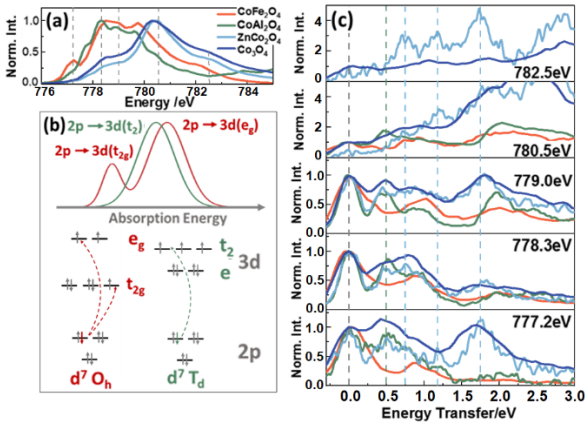

Fig. 1 Experimental cobalt (a) L_3-edge XAS and (c) 2p3d RIXS of $CoFe_2O_4$, $CoAl_2O_4$, $ZnCo_2O_4$ and Co_3O_4 at different incident energy (c) Schematic L_3-edge XAS of free ion with d^7 in O_h and T_d symmetry.

The combination of experimental and calculated spectra, shows that the transition at 0.5 eV energy transfer (at 779 eV incident energy) corresponds primarily to the $Co^{2+}(T_d)$ site. Figure 3 shows that the electronic structure of the $Co^{2+}(T_d)$ is sensitive to the amount of Fe loading. The sample with the lowest Fe loading, $Co_{2.95}Fe_{0.05}O_4$, exhibits an increase in the energy transfer, compared to the pristine Co sample, while Co_2FeO_4 with higher Fe incorporation shows a shift towards lower ET. This observation suggests a higher crystal field splitting for the sample with less Fe-loading, which interestingly correlates with a lower potential for the oxidation of the $Co^{2+}(T_d)$ site observed in cyclic voltammetry measurements. The opposite effect is observed for the Co_2FeO_4, indicating that this feature can be used to provide an electronic explanation for Fe-induced changes observed in electrocatalytic measurements, where the samples with the lowest Fe-loading showed enhanced electrocatalytic water oxidation performance.

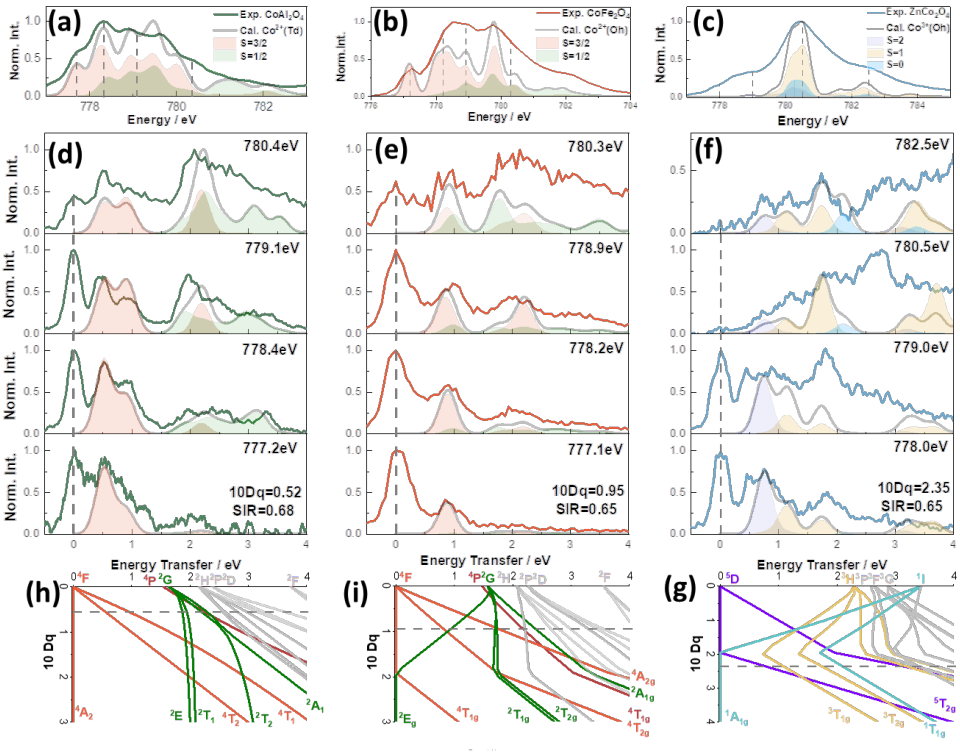

Fig.2 Experimental and ligand-field multiplet calculated L_3-edge XAS and 2p3d RIXS, as well as calculated Tanabe-Sugano diagrams of (a, d, g) $CoAl_2O_4$, (b, e, h.) $CoFe_2O_4$, and (c, f, i) $ZnCo_2O_4$.

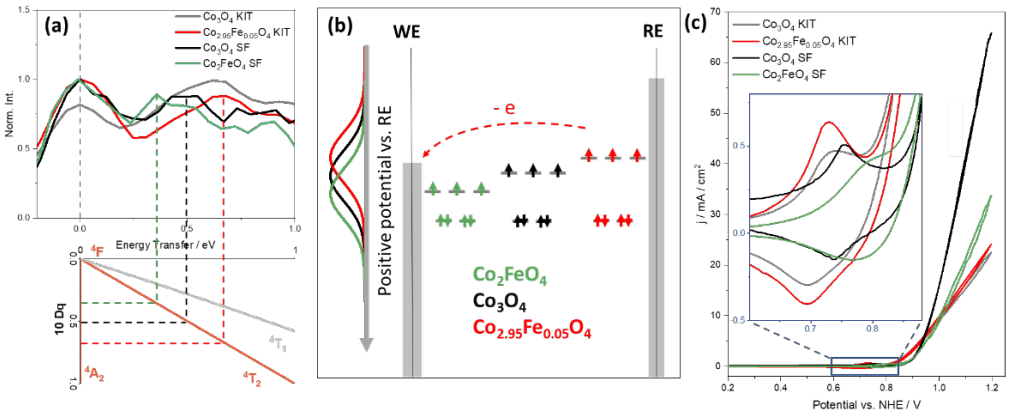

Fig. 3 (a) 2p3d RIXS show ligand field splitting of $Co^{2+}(T_d)$ affected by Fe loading. (b) Schematic diagram of relationship between 10Dq and oxidation potential. (c) Comparison of OER performance and the corresponding enlarged pre-catalytic redox couple of Co_3O_4 $Co_{2.95}Fe_{0.05}O_4$ and Co_2FeO_4.

References

[1] X. Deng, H. Tüysüz, et al, Chem. Mater., 2017, 29, 40−52.
[2] R. P. Wang, F. de Groot, J. Phys. Chem. C 2022, 126, 8752−8759.
[3] F. Neese, WIREs Computational Molecular Science 2011, 2, 73-78.